Estimating Short-Period Dynamics Using an Extended Kalman Filter

Jeffrey E. Bauer and Dominick Andrisani

June 1990

NASA

National Aeronautics and
Space Administration

Estimating Short-Period Dynamics Using an Extended Kalman Filter

Jeffrey E. Bauer
Ames Research Center, Dryden Flight Research Facility, Edwards, California

Dominick Andrisani
Department of Aeronautics and Astronautics, Purdue University, West Lafayette, Indiana

1990

ESTIMATING SHORT-PERIOD DYNAMICS USING AN EXTENDED KALMAN FILTER

Jeffrey E. Bauer*
NASA Ames Research Center
Dryden Flight Research Facility
Edwards, California
and
Dominick Andrisani**
Department of Aeronautics and Astronautics
Purdue Unversity
West Lafayette, Indiana

Abstract

In this paper, an extended Kalman filter (EKF) is used to estimate the parameters of a low-order model from aircraft transient response data. The low-order model is a state space model derived from the short-period approximation of the longitudinal aircraft dynamics. The model corresponds to the pitch rate to stick force transfer function currently used in flying qualities analysis. Because of the model chosen, handling qualities information is also obtained. The parameters are estimated from flight data as well as from a six-degree-of-freedom, non-linear simulation of the aircraft. These two estimates are then compared and the discrepancies noted. The low-order model is able to satisfactorily match both flight data and simulation data from a high-order computer simulation. The parameters obtained from the EKF analysis of flight data are compared to those obtained using frequency response analysis of the flight data. Time delays and damping ratios are compared and are in agreement. This technique demonstrates the potential to determine, in near real time, the extent of differences between computer models and the actual aircraft. Precise knowledge of these differences can help to determine the flying qualities of a test aircraft and lead to more efficient envelope expansion.

---

*Aerospace Engineer. Member AIAA.
**Professor. Member AIAA.

Nomenclature

d	distance from angle-of-attack vane to aircraft center of gravity
EKF	extended Kalman filter
$F(x,t)$	linearization of f about x at time t
$f(x,t)$	nonlinear function dependent on variable x at time t
g	gravitational constant
H	linearized output matrix, defined in equation (22)
h	nonlinear output matrix
I	identity matrix
K	Kalman gain matrix
L_q	derivative of $\dot{\alpha}$ with respect to q
L_α	derivative of $\dot{\alpha}$ with respect to α
L_δ	derivative of $\dot{\alpha}$ with respect to δ
LOES	low-order equivalent system
M_q	dimensional variation of pitching moment with pitch rate
M_α	dimensional variation of pitching moment with angle of attack
M_δ	dimensional variation of pitching moment with surface deflection
n_z	normal acceleration
P	Riccati error covariance
Q	model noise variance (process noise)
q	pitch rate
R	measurement noise variance

V	velocity
v	measurement noise
x	state vector
$\hat{x}_k(+)$	estimate of x taking advantage measured data at k
$\hat{x}_k(-)$	estimate of x before measured data at k is available
z	output vector
α	angle of attack
δ	pseudo control surface deflection
δ_p	pilot pitch stick signal
ρ	correlation coefficient
σ	standard deviation
τ	first-order time lag coefficient
τ_d	pure time delay
ω	process noise
$\omega_{n_{sp}}$	short-period natural frequency

Subscripts

c	corrected
f	flight measured
k	at discrete time k
m	measured parameter
0	initial

Superscript

T	matrix transpose operator
$\char`\^$	estimate

Introduction

Many near-real-time techniques have been used in the envelope expansion of recent research aircraft like the X-29.[1] In the area of flight controls, two real-time techniques were developed. One is a frequency response technique[2] where the aircraft's open-loop frequency response is determined from measured flight parameters. This frequency response is then compared with a predicted frequency response based on the current aircraft simulation. The second technique is a time history overplot comparison,[3] conducted in real time. Overplots are obtained of the aircraft response with time histories generated from a previously determined linear model of the aircraft, at that flight condition, driven by the pilot's input signal as it is telemetered to the ground.

To provide more detailed information, an additional real-time technique, the subject of this paper, has been investigated. This technique uses an extended Kalman filter (EKF) to estimate a low-order equivalent system (LOES) model of the aircraft from flight-measured time histories. References 4–9 detail other work in this area. For other work in parameter estimation see Refs. 10 and 11.

A Kalman filter is an optimal state estimator of a linear system. The estimate is adjusted based on each measurement of the system. An extended Kalman filter extends linear Kalman filter theory to nonlinear systems.

The LOES model is based on the longitudinal short-period approximation in the MIL-STD-1797 for flying qualities.[12] This technique is able to extract flying qualities parameters in near real time, which may quantify discrepancies between the aircraft and the aircraft simulation.

Before the flight, the aircraft's six-degree-of-freedom, nonlinear simulation is analyzed at a specified flight condition, and a LOES is estimated. During flight test, parameters of the low-order model are estimated and these flight-data based estimates are compared with the simulation based estimates in real time. The results of the flight estimation are intended to help diagnose discrepancies between the aircraft response and the predicted response. This comparison could be done before the aircraft reaches its next test point, giving the flight controller time to decide whether the discrepancy is serious enough to curtail further testing.

The aircraft used in developing this technique was the X-29 (Fig. 1). The X-29 airframe has a negative static margin of approximately 35 percent. This instability requires a high degree of control augmentation. The control system is entirely fly-by-wire, consisting of a triply redundant primary channel operating at 80 Hz. The longitudinal control laws use pitch rate and normal acceleration feedbacks for primary stability and control. Of particular importance to the EKF algorithm is the airplane's three surface pitch control, using canards, symmetric flaps, and strake flaps. Data from the airplane is telemetered to the control room at 40 samples/sec (40 Hz).

The estimation was made of the closed-loop system rather than the open-loop system. Because of the high degree of control augmentation on the X-29, the researchers thought that estimating the closed-loop system offered the best chance of success. The control

system was designed to make the closed-loop aircraft behave much like the low-order model. Detailed postflight analysis would provide greater insight into any discrepancy by separating the effects of the control system from the aerodynamics.

If a major discrepancy between the simulation and actual airplane is present, this algorithm may be able to determine what the discrepancy is more quickly than currently available technology can.

Not only general information about the aircraft performance, compared to its predicted performance, is available, but handling qualities data is obtained as well. First, an equivalent time delay is available. This value can be monitored to identify potential stability problems. The time delay computed in near real time would be used to identify large discrepancies from the anticipated values.

In addition, plots of normal acceleration divided by angle of attack (n_z/α) could be obtained for both the simulation and real-time estimations. This would allow researchers to determine if the flight values are moving towards an unacceptable region as defined by Ref. 12.

With the information provided by this technique in near real time, more intelligent decisions about the ongoing flight test could be made, possibly saving time and money. The results obtained by this technique could also increase the efficiency and safety of the flight test program.

The potential for reducing postflight data processing is also great. This technique could determine the area responsible for any discrepancies, and postflight analysis could then identify the cause.

Techniques and Procedures

Modeling

Only the transient longitudinal dynamics of the aircraft in 1-g level flight are studied. The basic model is the longitudinal short-period approximation

$$\dot{\alpha} = L_\alpha \alpha + L_q q + L_\delta \delta \qquad (1)$$

$$\dot{q} = M_\alpha \alpha + M_q q + M_\delta \delta \qquad (2)$$

where L_α, L_q, and L_δ are the derivatives of $\dot{\alpha}$ with respect to α, q, and δ, and M_α, M_q, and M_δ are the derivatives of $\dot{q}$ with respect to α, q, and δ. This approximation is equivalent to the short-period approximation for the pitch rate to stick force transfer function given in Ref. 12, allowing handling qualities informa-

tion to be obtained. Aircraft angle of attack, pitch rate, and normal acceleration make up the systems observation equations.

Because of the aircraft's open-loop instability, the closed-loop dynamics were estimated rather than the open-loop dynamics. If the open-loop equations were used, then any small measurement errors in the surface positions or the numerical differentiation would cause the model to diverge from the measurements.

The aircraft uses three surfaces for pitch control. This configuration made defining a stick force to aircraft response transfer function difficult. Since there was no single pitch generating surface, the effects of the three surfaces were collected into a single pseudo control surface. A third state equation is added to the model to represent the pseudo control

$$\dot{\delta}(t) = \frac{-1}{\tau}\delta(t) + \frac{-1}{\tau}\delta_p(t - \tau_d) \qquad (3)$$

where δ is the pseudo control surface deflection and δ_p is the pilot pitch stick signal. It was reasoned that this equation should have the appearance of an actuator model. The coefficient of the model is estimated by the filter. Equation (3) contains a first-order lag of the pilot's stick signal. The first-order lag accounts for only part of the system time delay. The rest is modeled through a pure time delay.[13]

To determine the pure time delay, several *a priori* estimates are made, and several filters are run in parallel. To determine which of these filters is operating with the proper amount of pure time delay, the likelihood function is used.[14] The proper amount of pure time delay is the sum of each filter's time delay multiplied by its likelihood. However, in all cases examined one delay always resulted in a likelihood much higher than the others. For this reason, and to save computational complexity, the time delay associated with the largest likelihood is used as the correct pure time delay. Figure 2 shows that the pure time delay is implemented outside of the EKF.

A detailed investigation of identifiability was not conducted. However, the fact that one delay resulted in a likelihood far larger than the others suggested identifiabilty is not a problem.

Since the aircraft cannot obtain perfect trim in flight, estimated bias terms are added to the state equations. In the presence of trim errors these terms balance the state equations and accurately determine the trim state. Without the biases, the equations would integrate a small error over the course of the maneuver.

3

The equation for measured angle of attack needs to be corrected for the fact that angle of attack is measured at the noseboom of the aircraft and not the center of gravity. This can be modeled to the first order by correcting for pitch rate

$$\alpha_m = \alpha - \frac{d}{V}q \qquad (4)$$

where α_m is the measured angle of attack and d is the distance from the angle-of-attack vane to the aircraft center of gravity.

The equivalent system model can now be defined and is given by equations (5–10)

$$\dot{\alpha} = L_\alpha \alpha + L_q q + L_\delta \delta + L_0 \qquad (5)$$

$$\dot{q} = M_\alpha \alpha + M_q q + M_\delta \delta + M_0 \qquad (6)$$

$$\dot{\delta} = \frac{-1}{\tau}\delta + \frac{-1}{\tau}\delta_p + \delta_0 \qquad (7)$$

$$\alpha_m = \alpha - \frac{d}{V}q \qquad (8)$$

$$q_m = q \qquad (9)$$

$$n_{z_m} = \frac{-V}{g}[L_\alpha \alpha + (L_q - 1)q$$
$$+ L_\delta \delta + L_0] + n_{z_0} \qquad (10)$$

where the subscript 0 indicates initial state.

Estimation

The estimation problem consists of estimating L_α, L_q, L_δ, M_α, M_q, M_δ, $\frac{1}{\tau}$, L_0, M_0, δ_0, n_{z_0} of the longitudinal short-period approximation model as a function of time for the closed-loop aircraft response, in near real time. To do this using an EKF, these coefficients must be made states of the filter. Therefore the state vector (x) becomes

$$x = [\alpha, q, \delta, L_\alpha, M_\alpha, L_\delta, M_\delta, L_q,$$

$$M_q, \frac{1}{\tau}, L_0, M_0, \delta_0, n_{z_0}]^T \qquad (11)$$

The extra state equations required are $\dot{L}_\alpha = 0$, $\dot{M}_\alpha = 0$, $\dot{L}_\delta = 0$, $\dot{M}_\delta = 0$, $\dot{L}_q = 0$, $\dot{M}_q = 0$, $(\frac{1}{\tau}) = 0$, $\dot{L}_0 = 0$, $\dot{M}_0 = 0$, $\dot{\delta}_0 = 0$, and $\dot{n}_{z_0} = 0$. The short-period state equations (5–7), augmented by those previously listed and output equations (8–10), form the state and measurement equations for the EKF.

The EKF equations used are for a continuous-discrete system and are listed in the following equations.[15]

The continuous system model is

$$\dot{x}(t) = f(x(t), t) + \omega(t) \qquad (12)$$

where ω is a white noise process with spectral density $Q(t)$ where Q is the model noise variance.

The discrete measurement model is

$$z_k = h_k(x(t_k)) + \nu_k \quad ; \quad k = 1, 2, 3, \dots \qquad (13)$$

where the ν_k's are independent Gaussian noise vectors with mean zero and covariance R_k. It is also assumed that ω and ν are independent.

The initial conditions are

$$x(0) \qquad (14)$$

where $x(0)$ is Gaussian, with mean $\hat{x}_0$ and variance P_0.

The state estimate propagation between samples is

$$\dot{\hat{x}}(t) = f(\hat{x}(t), t) \qquad (15)$$

The error covariance propagation between samples is

$$\dot{P}(t) = F(\hat{x}(t), t)P(t)$$
$$+ P(t)F^T(\hat{x}(t), t) + Q(t) \qquad (16)$$

where $P(t)$ is the Ricatti error covariance, and $F(\hat{x}(t), t)$ is defined in equation (20).

The state estimate update is

$$\hat{x}_k(+) = \hat{x}_k(-) + K_k[z_k - h_k(\hat{x}_k(-))] \qquad (17)$$

where (+) is the estimate using information at time k, (−) is the estimate before data from time k is available, and K is the Kalman gain matrix defined in equation (19).

The error covariance update is

$$P_k(+) = [I - K_k H_k(\hat{x}_k(-))]P_k(-) \qquad (18)$$

where $H_k(\hat{x}_k(-))$ is defined in equation (21).

The Kalman gain matrix is

$$K_k = P_k(-)H_k^T(\hat{x}_k(-))$$

$$[H_k(\hat{x}(-))P_k(-)H_k^T$$

$$(\hat{x}_k(-)) + R_k]^{-1} \qquad (19)$$

4

Definitions

$$F(\hat{x}(t), t) = \left. \frac{\partial f(x(t), t)}{\partial x(t)} \right|_{x(t) = \hat{x}(t)} \qquad (20)$$

$$H_k(\hat{x}_k(-)) = \left. \frac{\partial h_k(x(t_k))}{\partial x(t_k)} \right|_{x(t_k) = \hat{x}_k(-)} \qquad (21)$$

Equation (12) for the system model is a continuous nonlinear equation describing the state propagation with time, between samples. An approximation that F is constant between samples has been made. In this application, the state is propagated through the nonlinear equations using a fourth-order Runge-Kutta technique. The measurement model (equation (13)) is discrete. In equation (20), F is the linearized state matrix. This matrix must be recomputed for each update of the state vector since the elements of F are also states of the EKF and will change with each update of the filter.

The first step in estimating the flight data is obtaining an estimate from the simulation. There are two primary objectives in estimating the low-order model from nonlinear simulation data. First, determine the coefficients of the low-order model (filter states 4–11) as accurately as possible. These will be the initial state estimates for the estimation from the flight data. In addition, the simulation estimates will be compared to the estimates obtained from the flight data to check for major discrepancies.

The second objective is to determine the amount of process noise to use in estimating the data from flight. For the X-29A, earlier flight tests have shown that the nonlinear simulation accurately predicts the response of the airplane. As a result, the process noise weighting matrix is selected by adjusting the weighting matrix until both the EKF and LOES indicated that good results had been obtained. Overplots of the LOES system with the original data are used to evaluate the estimates qualitatively. Innovations, time histories of the estimates, correlations, and state variances from the EKF are used in the evaluation. A tradeoff is then made between the EKF and LOES results to obtain the final estimates and weightings. These weightings are then used to estimate the parameters during flight. In the cases examined, the process noise weightings were kept quite low.[16]

To determine values for the measurement noise (R), sample time histories are obtained. From these, bounds are drawn defining a noise envelope for that signal. These bounds are then selected as $\pm 2\sigma$ (two standard deviations) bounds about the mean. The value for $R_{i,i}$ in this case is $\sigma_{i,i}^2$. This is possible because the process noise was kept low.

For α and q, the initial state variance ($P(0)$) is the value for measurement noise on α and q. For the other states a value for σ is selected which equals one-fourth the estimated initial values of the states, thus $P_{i,i} = \hat{\sigma}_{i,i}^2 = (\frac{1}{4}\hat{x}_{i,i})^2$. For state variables with initial values close or equal to zero, bounds are established based on engineering judgement.

With the identification algorithm initialized, the next step is to determine the pure time delay. Nine filters are run with fixed time delays ranging from 0 to 200 msec, in increments of 25 msec. The likelihood function is used to determine which filter is operating with the correct amount of time delay.

Several analysis techniques are used to monitor the filter and to aid in interpreting the results. The most important of these are the filter innovations. The innovations are the difference between the predicted output of the equivalent system and the measured response. The innovations are calculated by

$$\text{innovations} = z_k - h_k(x_k(-)) \qquad (22)$$

Results and Discussion

Simulation

A simulation time history is generated using the six-degree-of-freedom, nonlinear simulation and flight data inputs at this condition. Some of the flight data analyzed is presented in Fig. 3. The actual time interval of the identification was varied to illustrate various points.

The filter is initialized as described earlier. The measurement noise is determined from the flight data and then divided by 100 (to represent $\frac{1}{10}$ the root mean square error) since the simulation would produce a perfect measurement signal. A low-order equivalent system is then estimated from this data. The results of this estimation are presented in Table 1.

Large correlations between the state δ and the coefficients M_0 and δ_0 are found. Some correlation is also indicated between the coefficients M_q and M_δ. This is expected because the control system has the appearance of a pitch rate command system. Although this correlation is not desirable, it is not felt to be a problem.

5

These results are obtained for very low levels of process noise. Large values of process noise often result in misleading estimates. The values for final variance are much smaller than the initial values, which shows that the EKF has obtained a good estimate.

Plots of the LOES and the simulation time histories are shown in Fig. 4. The LOES matches the simulation data exceptionally well. The only discrepancy occurs between 9 and 10 sec. This discrepancy is believed to be the result of a nonlinearity around the zero stick position, possibly caused by break out forces or hysteresis in the stick at that point.

Flight

For the flight data estimation, the final results of the simulation estimation are used as the initial state estimates. The values for process noise are those determined from the simulation. The initial variance of the state is that used in the simulation estimation. The flight data is then processed to arrive at the final estimate, which is compared to the simulation final estimate. The output of the flight data estimation is presented in Table 2.

The same correlations among parameters that are seen on the simulation, δ with M_0 and δ_0, and M_δ with M_q, occur here. As before, this result is not desirable, but it is expected and is not thought to be a problem in the estimation.

Plots of the LOES and the flight data are presented in Fig. 5 and demonstrate excellent agreement with the flight data. However, for reasons which are not clear, the filter underestimates the final peak.

Figure 6 shows the innovations. The bounds of the innovations are obtained by the equation

$$\text{bound} = \pm 2[HPH^T + R]^{\frac{1}{2}}_{i,i} \qquad (23)$$

The structure, especially in the pitch rate data, indicates correlation over time because a low-order model was used to describe higher-order dynamics, resulting in process noise. This correlation also suggests that information is still available in the signal, or that the noise is not Gaussian and white. Additional tuning of the gains may reduce the correlation.

Figure 7 shows the time histories for the state estimates. In almost all cases, the states settle by approximately 9 sec. These results are encouraging. If the time histories for the states representing the parameter estimates vary wildly at the end of the estimation,

then little confidence could be held in the estimation for that state. Large variations would also be reflected in a large final variance for that state.

Simulation and Flight Comparisons

Figure 8 is a comparison of the final state estimates, with a $\pm 2\sigma$ error bound (based on the final P), of the simulation and flight estimations. The frequency and damping ratio are computed from the state estimates; their bounds were computed by a simple linearization. This is only an estimate of the bounds and is thought to be sufficient because of the low correlation of the parameters. The results were expected to agree better than they do.

The damping ratio is estimated to be higher from flight than from the simulation. This increased damping ratio has also been observed by the pilots and in postflight frequency response analysis. This increase in the damping ratio is also observed in the near-real-time open-loop frequency response analysis as an increase in the phase margin.

To further verify the results of the algorithm, the damping ratio and pure time delay estimates are compared to the results from the postflight frequency response analysis. The EKF estimated a time delay between 140 msec and 146 msec; the frequency response analysis estimated a time delay of 120 msec. For the damping ratio, the EKF estimated 0.84 to 0.92, the frequency response analysis estimated 1.05. The agreement is good, considering frequency and damping ratio tend to tradeoff without affecting performance.

Thus, the differences between the flight data estimates and the simulation data estimates are caused by a discrepancy between the simulation and airplane. Some discrepancies between the simulation and aircraft performance are expected. This demonstrates the EKF's ability to identify such discrepancies.

Robustness

The data was also analyzed in more detail to determine the robustness of the algorithm. In one instance, the window over which the estimation was performed was shifted 1.5 sec. This shift only has a slight effect on the final state estimates.

In another check for robustness, the filter was reinitialized with the final state estimate from the previous run and the process was repeated in an iterative fashion until convergence. Although the results differed slightly, they showed that the initial estimation would be sufficient. This is where the Kalman filter

6

possesses an advantage over other identification techniques, which require multiple processing of the data to obtain a final estimate. The results of the above two investigations are presented in Table 3.

The most dramatic evidence of the robustness of the algorithm, however, is its reaction to a data spike in the stick input signal at approximately 15 sec (Fig. 3(a)). This channel is the most sensitive to data spikes since the model in the filter algorithm will be driven by this input, producing outputs inconsistent with the aircraft outputs. As a result large differences between measured and predicted values can occur altering the state estimates unfavorably.

The flight data was estimated in the presence of this spike with the process noise weighting matrix equal to zero. The effects of this spike can be seen most clearly in the plots for the filter state (Fig. 9), at approximately 10.6 sec (the difference in time is due to the window over which the flight data is identified). The LOES model and flight data (Fig. 10) still agree well especially considering that the process noise was zero. The ability of the algorithm to survive a data spike of such magnitude on the most critical channel indicates that the algorithm will perform well during flight test.

Since the technique is in the developmental stage all the analysis so far has been postflight analysis. The goal of this technique is implementation during flight test. While proving the concept, however, execution speed was not considered. Once the technique was proven sound and acceptable, computation time was considered. By then, there was time for only a cursory investigation. The resulting execution time was approximately 2.5 min (central processing unit (cpu) time) to process 10 sec of flight data. Major sections of the code may be written more efficiently, reducing the execution time. When the program is moved to the computer used during flight test, faster computation times may occur because of the increased capabilities of this system.

Concluding Remarks

A third-order model based on the short-period approximation is an acceptable model to describe the pitch axis transient response of highly augmented and very large order aircraft dynamics. This equivalent system model can be estimated by using an extended Kalman filter. Results suggest such an estimation could be conducted in near real time during flight test.

The results of this technique have been verified against the existing near-real-time open-loop frequency response analysis and postflight frequency domain handling qualities analysis.

The ability to determine equivalent time delay, undamped natural frequency, and damping ratio in near real time provides the flight test organization with quick and accurate information about the aircraft, contributing to safe, quick, and efficient flight testing.

References

[1] Hicks, John W., and Kevin L. Petersen, "Real-Time Flight Test Analysis and Display Techniques for the X-29A Aircraft," paper number 6, AGARD 73rd Flight Test Techniques Symposium, Flight Mechanics Panel, Oct. 17–20, 1988.

[2] Bosworth, J.T., and J.C. West, "Real-Time Open-Loop Frequency Response Analysis of Flight Test Data," AIAA 86-9738, Apr. 1986.

[3] Bauer, Jeffrey E., David B. Crawford, Joseph Gera, and Dominick Andrisani, II, "Real-Time Comparison of X-29A Flight Data and Simulation Data," AIAA 87-0344, Jan. 1987. Also available in *J. Aircraft*, vol. 26, no. 2, Feb. 1989.

[4] Pischoff, David E., "Longitudinal Equivalent Systems Analysis of Navy Tactical Aircraft," AIAA 81-1775, Aug. 1981.

[5] Burton R.A., B.T. Kneeland, U.H. Rabin, and R.S. Hansen, "Flight Testing and Development of the F/A-18A Digital Flight Control System," *Active Control Systems*, RTP# AGARD-CP-384, 1985.

[6] Speyer, Jason L., and Edwin Z. Crues, "On-Line Aircraft State and Stability Derivative Estimation Using the Modified-Gain Extended Kalman Filter," *J. Guidance*, vol. 10, no. 3. Also available as AIAA 85-1762.

[7] Klein, Vladislav, and James R. Schiess, *Compatibility Check of Measured Aircraft Responses Using Kinematic Equations and Extended Kalman Filter*, NASA TN D-8514, 1977.

[8] Kain, J.E., C.M. Brown, Jr., J.G. Lee, S. Pallas, and E.S. Sears, "Missile Aerodynamic Parameter and Structure Identification from Flight Test Data," AIAA 78-1341, Aug. 1978.

[9] Kain, J.E., "An Evaluation of Aeroballistic Range Projectile Parameter Identification Procedures," AIAA 79-1687, Aug. 1979.

[10] Maine, Richard E., and Kenneth W. Iliff, *Identification of Dynamic Systems. Theory and Formulation*, NASA RP-1138, 1985.

[11] Maine, Richard E., and Kenneth W. Iliff, *Application of Parameter Estimation to Aircraft Stability and Control. The Output-Error Approach*, NASA RP-1168, 1986.

[12] *Flying Qualities for Piloted Vehicles*, MIL-STD-1797 (USAF) 1987.

[13] Shafer, M.F., "Low-Order Equivalent Models of Highly Augmented Aircraft Determined from Flight Data," *J. Guidance, Control, and Dynamics*, vol. 5, no. 5, Sept.–Oct. 1982, p. 504. Also available as AIAA 80-1627-R.

[14] Andrisani, D., *Multipartitioned Estimation Algorithms*, Ph.D. dissertation, State University of New York at Buffalo, 1978.

[15] Gelb, Arthur, ed., *Applied Optimal Estimation*, MIT Press, 1974.

[16] Bauer, J.E., *Identification of Equivalent Short Period Dynamics of the X-29A*, Masters Thesis, Purdue University, Dec. 1988.

Table 1. Output for simulation identification.

(Undamped natural frequency = 4.2596; damping ratio = 0.5753)

Vector	Output Data						
	α	q	δ	L_α	M_α	L_δ	M_δ
Initial state estimate	0.000×10^0	0.000×10^0	0.000×10^0	-0.191×10^1	-0.140×10^2	0.130×10^{-3}	-0.377×10^0
Final state estimate	0.505×10^{-2}	-0.171×10^{-1}	0.706×10^{-1}	-0.191×10^1	-0.124×10^2	-0.249×10^{-4}	-0.317×10^0
Initial variance	0.116×10^{-5}	0.119×10^{-5}	0.100×10^{-3}	0.112×10^0	0.536×10^1	0.625×10^{-3}	0.596×10^{-2}
Final variance	0.404×10^{-9}	0.420×10^{-7}	0.212×10^{-4}	0.385×10^{-5}	0.113×10^{-1}	0.679×10^{-9}	0.120×10^{-4}
Measurement noise variance	---	---	---	---	---	0.382×10^{-3}	0.391×10^{-3}
State noise estimate	0.000×10^1	0.500×10^{-4}	0.000×10^0	0.000×10^0	0.000×10^0	0.000×10^0	0.000×10^0

Vector	Output Data					
	L_q	M_q	$1/\tau$	L_0	M_0	δ_0
Initial state estimate	0.101×10^1	-0.368×10^1	0.792×10^1	0.000×10^0	0.000×10^0	0.000×10^0
Final state estimate	0.101×10^1	-0.299×10^1	0.106×10^2	-0.486×10^{-3}	0.187×10^{-1}	0.783×10^0
Initial variance	0.100×10^{-1}	0.266×10^1	0.156×10^1	0.100×10^{-3}	0.100×10^{-1}	0.225×10^1
Final variance	0.280×10^{-6}	0.244×10^{-2}	0.209×10^{-1}	0.822×10^{-9}	0.303×10^{-5}	0.232×10^{-2}
Measurement noise variance	0.138×10^{-5}	---	---	---	---	---
State noise estimate	0.000×10^0	0.000×10^0	0.000×10^0	0.000×10^0	0.000×10^0	0.000×10^0

Table 1. Concluded.

The Correlation Coefficient Matrix

	α	q	δ	L_α	M_α	L_δ	M_δ	L_q	M_q	$1/\tau$	L_0	M_0	δ_0
α	1.00000	0.15506	−0.24955	0.41331	0.06827	−0.32304	0.08508	−0.39590	0.10736	0.07459	0.74554	−0.17110	−0.24041
q	0.15506	1.00000	0.05098	−0.06954	0.04102	0.03762	−0.07725	0.03875	−0.10829	−0.03979	−0.01686	0.06768	0.04516
δ	−0.24955	0.05098	1.00000	−0.02653	−0.00236	0.11107	−0.14909	0.06080	−0.12547	−0.15092	−0.34409	0.96273	0.98721
L_α	0.41331	−0.06954	−0.02653	1.00000	0.01610	−0.48989	0.08355	−0.59820	0.19205	0.06850	0.00178	−0.04350	−0.01579
M_α	0.06827	0.04102	−0.00236	0.01610	1.00000	−0.12624	0.54708	−0.09847	0.34516	0.73953	0.01722	−0.12007	0.11690
L_δ	−0.32304	0.03762	0.11107	−0.48989	−0.12624	1.00000	−0.22689	0.77509	−0.21938	−0.16148	−0.07766	0.14283	0.08631
M_δ	0.08508	−0.07725	−0.14909	0.08355	0.54708	−0.22689	1.00000	−0.17641	0.92781	0.84812	0.07540	−0.31789	−0.01402
L_q	−0.39590	0.03875	0.06080	−0.59820	−0.09847	0.77509	−0.17641	1.00000	−0.20940	−0.04785	−0.05120	0.08488	0.05378
M_q	0.10736	−0.10829	−0.12547	0.19205	0.34516	−0.21938	0.92781	−0.20940	1.00000	0.73248	0.06831	−0.28246	−0.00877
$1/\tau$	0.07459	−0.03979	−0.15092	0.06850	0.73953	−0.16148	0.84812	−0.04785	0.73248	1.00000	0.07437	−0.30871	0.00863
L_0	0.74554	−0.01686	−0.34409	0.00178	0.01722	−0.07766	0.07540	−0.05120	0.06831	0.07437	1.00000	−0.23452	−0.33607
M_0	−0.17110	0.06768	0.96273	−0.04350	−0.12007	0.14283	−0.31789	0.08488	−0.28246	−0.30871	−0.23452	1.00000	0.92405
δ_0	−0.24041	0.04516	0.98721	−0.01579	0.11690	0.08631	−0.01402	0.05378	−0.00877	0.00863	−0.33607	0.92405	1.00000

10

Table 2. Output for flight data identification.

(Undamped natural frequency = 4.6965; damping ratio = 0.8823)

Vector	Output Data						
	α	q	δ	L_α	M_α	L_δ	M_δ
Initial state estimate	0.000×10^0	0.000×10^0	0.000×10^0	-0.191×10^1	-0.124×10^2	-0.249×10^{-4}	-0.317×10^0
Final state estimate	0.553×10^{-2}	-0.611×10^{-2}	0.261×10^{-1}	-0.210×10^1	-0.895×10^1	-0.342×10^{-4}	-0.367×10^0
Initial variance	0.116×10^{-5}	0.119×10^{-5}	0.100×10^{-3}	0.112×10^0	0.536×10^1	0.625×10^{-3}	0.596×10^{-2}
Final variance	0.297×10^{-8}	0.874×10^{-7}	0.122×10^{-4}	0.725×10^{-4}	0.247×10^{-1}	0.746×10^{-8}	0.492×10^{-4}
Measurement noise variance	---	---	---	---	---	0.382×10^{-2}	0.391×10^{-2}
State noise estimate	0.000×10^0	0.500×10^{-4}	0.000×10^0	0.000×10^0	0.000×10^0	0.000×10^0	0.000×10^0

Vector	Output Data					
	L_q	M_q	$1/\tau$	L_0	M_0	δ_0
Initial state estimate	0.101×10^1	-0.299×10^1	0.106×10^2	0.000×10^0	0.000×10^0	0.000×10^0
Final state estimate	0.101×10^1	-0.619×10^1	0.146×10^2	-0.690×10^{-4}	0.944×10^{-2}	0.402×10^0
Initial variance	0.100×10^{-1}	0.266×10^1	0.156×10^1	0.100×10^{-3}	0.100×10^{-1}	0.225×10^1
Final variance	0.595×10^{-5}	0.189×10^{-1}	0.891×10^{-1}	0.750×10^{-8}	0.245×10^{-5}	0.263×10^{-2}
Measurement noise variance	0.138×10^{-4}	---	---	---	---	---
State noise estimate	0.000×10^0	0.000×10^0	0.000×10^0	0.000×10^0	0.000×10^0	0.000×10^0

11

Table 2. Concluded.

The Correlation Coefficient Matrix

	α	q	δ	L_α	M_α	L_δ	M_δ	L_q	M_q	$1/\tau$	L_0	M_0	δ_0
α	1.00000	0.15520	0.30339	0.45422	0.00249	−0.32055	0.02536	−0.37004	0.08520	0.01546	0.75852	−0.48553	0.30227
q	0.15520	1.00000	0.01213	−0.19339	0.17469	0.09181	−0.08694	0.11508	−0.14395	−0.02172	0.03066	0.03982	0.00948
δ	0.30339	0.01213	1.00000	0.01650	0.03627	−0.02646	−0.00437	−0.02290	0.00088	0.02419	0.38338	0.92657	0.99320
L_α	0.45422	−0.19339	0.01650	1.00000	−0.15129	−0.52764	0.08438	−0.62633	0.23443	0.06157	−0.01968	0.00016	0.02351
M_α	0.00249	0.17469	0.03627	−0.15129	1.00000	−0.02030	0.46982	0.06861	0.32570	0.67047	−0.03501	−0.05660	0.11401
L_δ	−0.32055	0.09181	−0.02646	−0.52764	−0.02030	1.00000	−0.30411	0.86501	−0.34107	−0.13320	−0.02950	0.00150	−0.04172
M_δ	0.02536	−0.08694	−0.00437	0.08438	0.46982	−0.30411	1.00000	−0.22896	0.96893	0.87585	−0.04645	−0.13821	0.09768
L_q	−0.37004	0.11508	−0.02290	−0.62633	0.06861	0.86501	−0.22896	1.00000	−0.31818	0.01716	−0.01880	0.00127	−0.02069
M_q	0.08520	−0.14395	0.00088	0.23443	0.32570	−0.34107	0.96893	−0.31818	1.00000	0.81066	−0.04257	−0.12910	0.09529
$1/\tau$	0.01546	−0.02172	0.02419	0.06157	0.67047	−0.13320	0.87585	0.01716	0.81066	1.00000	−0.04749	−0.10711	0.14043
L_0	0.75852	0.03066	0.38338	−0.01968	−0.03501	−0.02950	−0.04645	−0.01880	−0.04257	−0.04749	1.00000	0.62764	0.37416
M_0	−0.48553	0.03982	0.92657	0.00016	−0.05660	0.00150	−0.13821	0.00127	−0.12910	−0.10711	0.62764	1.00000	0.90518
δ_0	0.30227	0.00948	0.99320	0.02351	0.11401	−0.04172	0.09768	−0.02069	0.09529	0.14043	0.37416	0.90518	1.00000

12

Table 3. Robustness investigation results.

Parameter	L_α	M_α	L_δ	M_δ	L_q	M_q	$1/\tau$	L_0	M_0	δ_0
Simulation	−1.91	−12.4	-2.49×10^{-5}	−0.317	1.01	−2.99	10.6	---	---	---
Flight data	−2.10	−8.95	-3.24×10^{-5}	−0.367	1.01	−6.19	14.6	-6.9×10^{-5}	9.44×10^{-3}	0.402
Time shift	−2.10	−8.42	-6.31×10^{-4}	−0.346	1.02	−5.76	16.8	2.34×10^{-5}	9.20×10^{-3}	4.62
Convergence	−2.09	−8.31	-2.66×10^{-5}	−0.370	1.01	−5.36	19.1	-4.75×10^{-5}	-2.22×10^{-3}	-8.73×10^{-2}
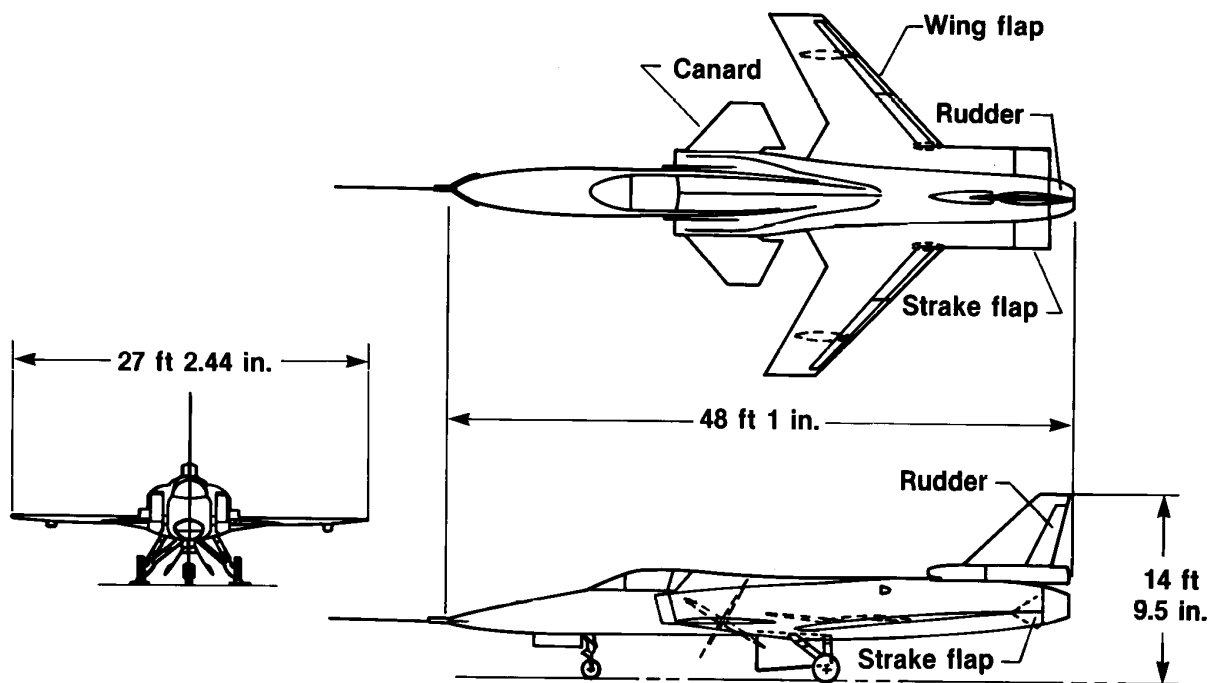
Fig. 1 The X-29A airplane.

900031
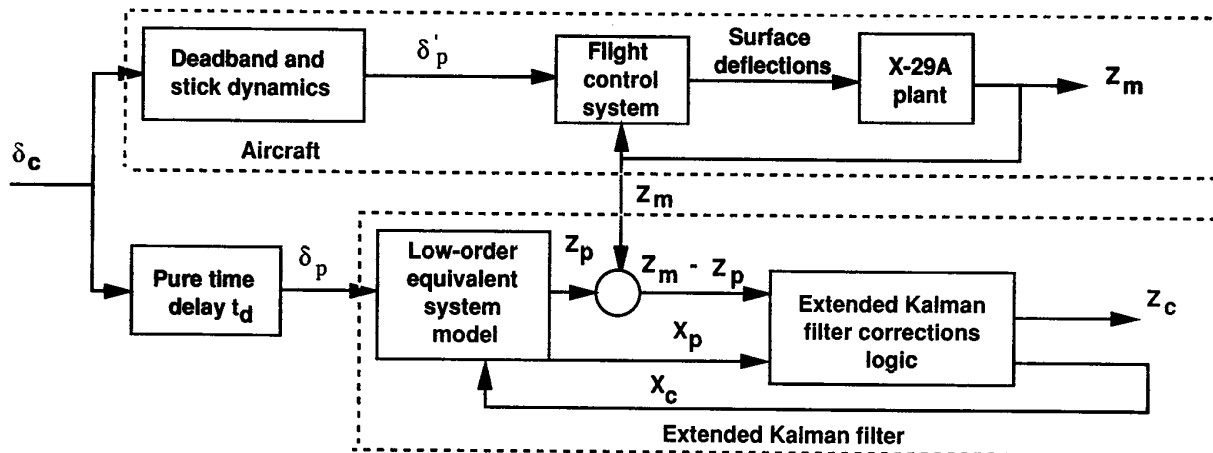
δ_c	Pilot command	z_c	Corrected angle of attack, pitch rate, and normal acceleration
δ'_p	Stick signal to flight control system		
δ_p	Stick signal used to drive extended Kalman filter aircraft model	z_p	Predicted angle of attack, pitch rate, and normal acceleration
z_m	Measured angle of attack, pitch rate, and normal acceleration	x_p	Predicted state vector
		x_c	Corrected state vector

900032

Fig. 2 Extended Kalman filter algorithm.

14
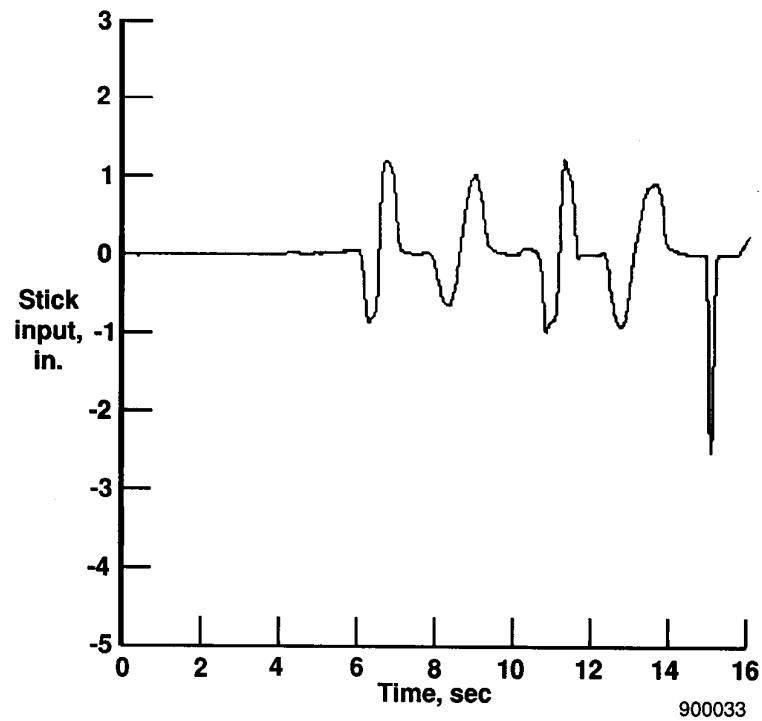
(a) Stick input.
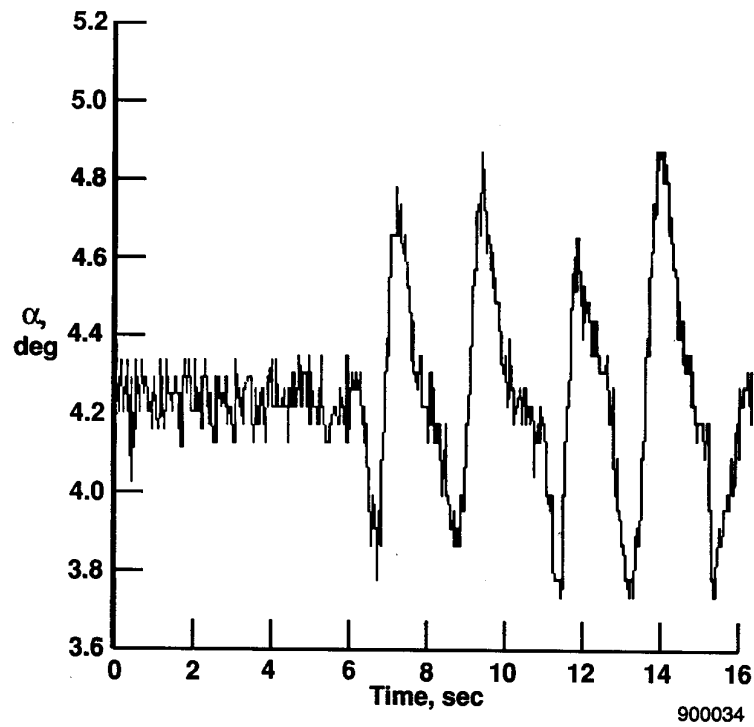
(b) Angle of attack.

Fig. 3 Flight data as a function of time.

15

900035

(c) Pitch rate.

900036
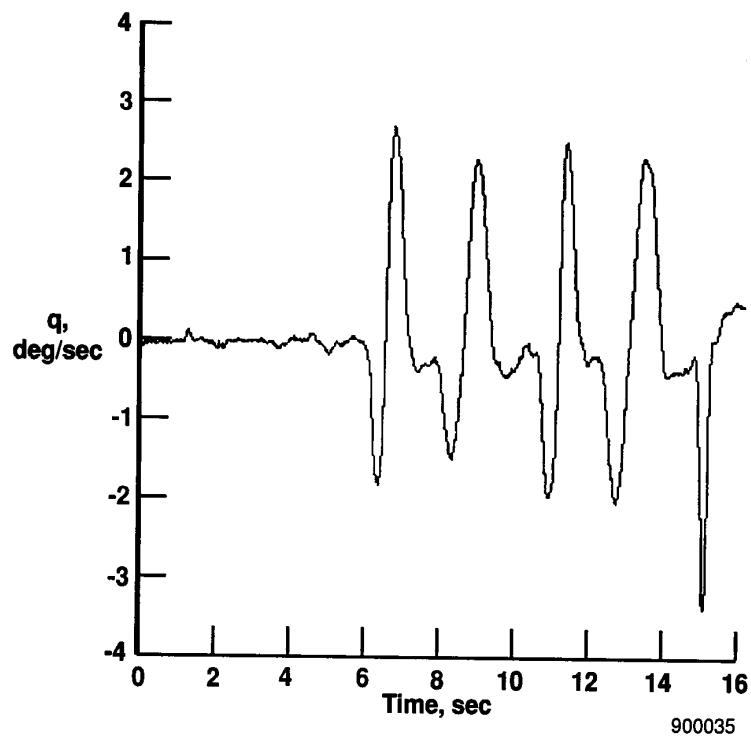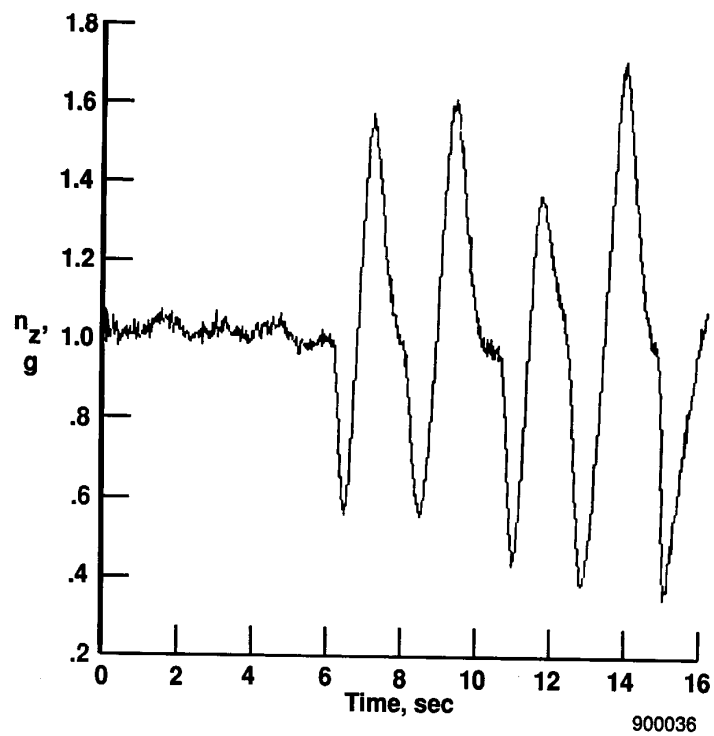
(d) Normal acceleration.

Fig. 3 Concluded.

16

(a) Angle of attack.

900037

(b) Pitch rate.

900038
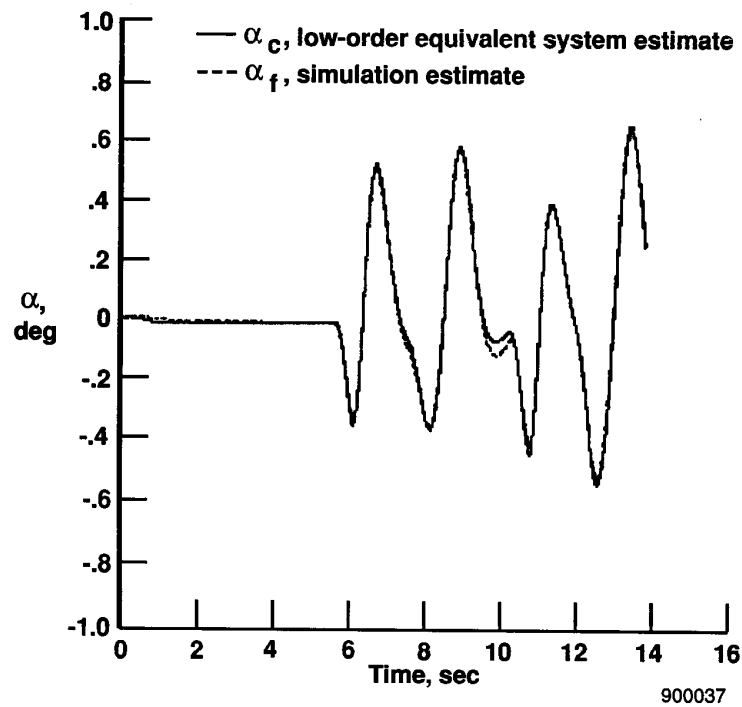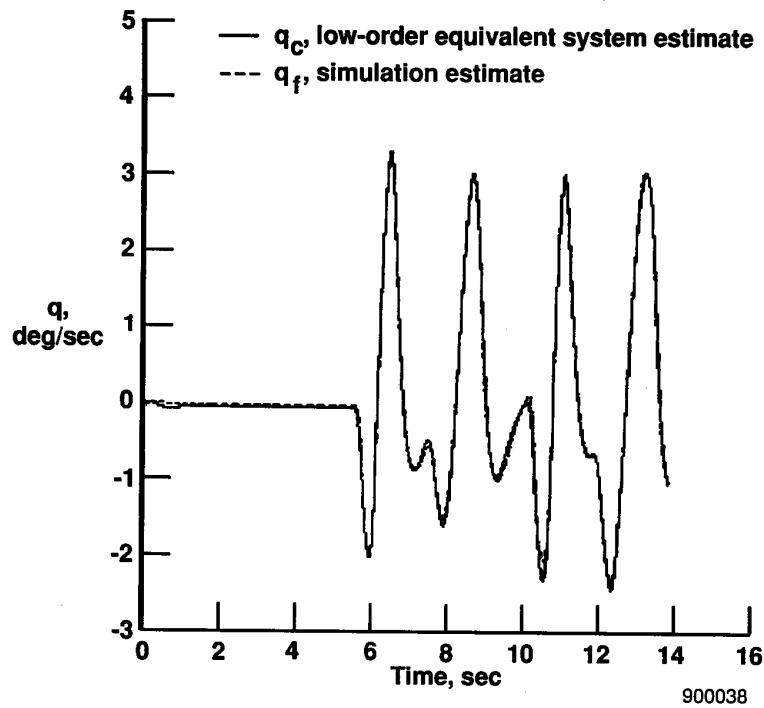
Fig. 4 Low-order equivalent system response compared with simulation data (perturbation quantities) as a function of time.
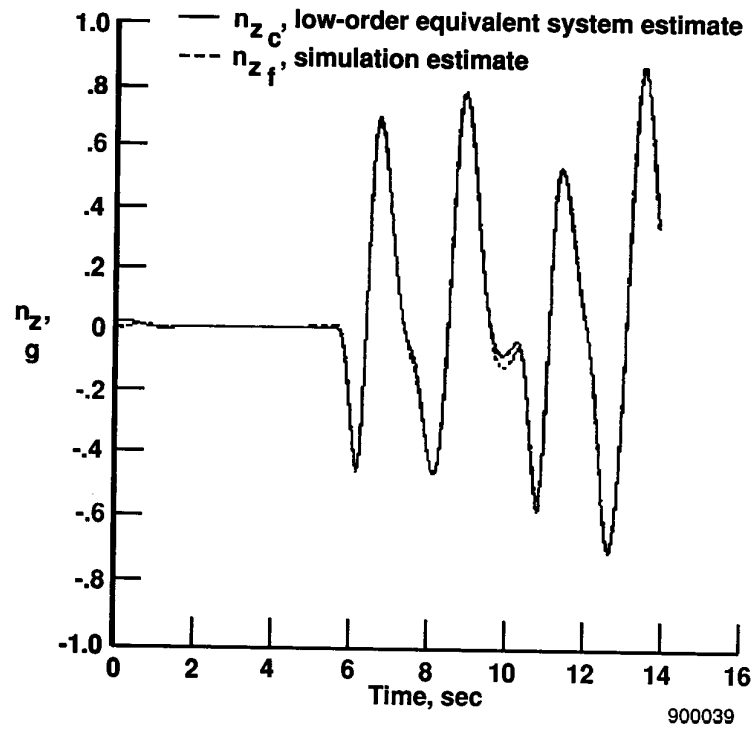
(c) Normal acceleration.

Fig. 4 Concluded.
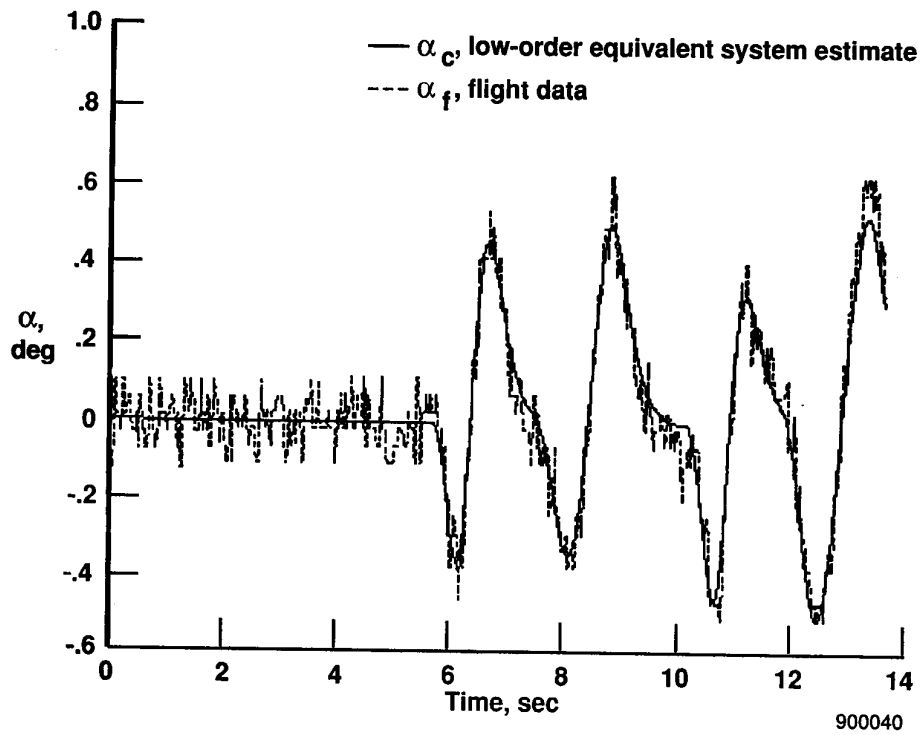
(a) Angle of attack.

Fig. 5 Low-order equivalent system response compared with flight data (perturbation quantities) as a function of time.
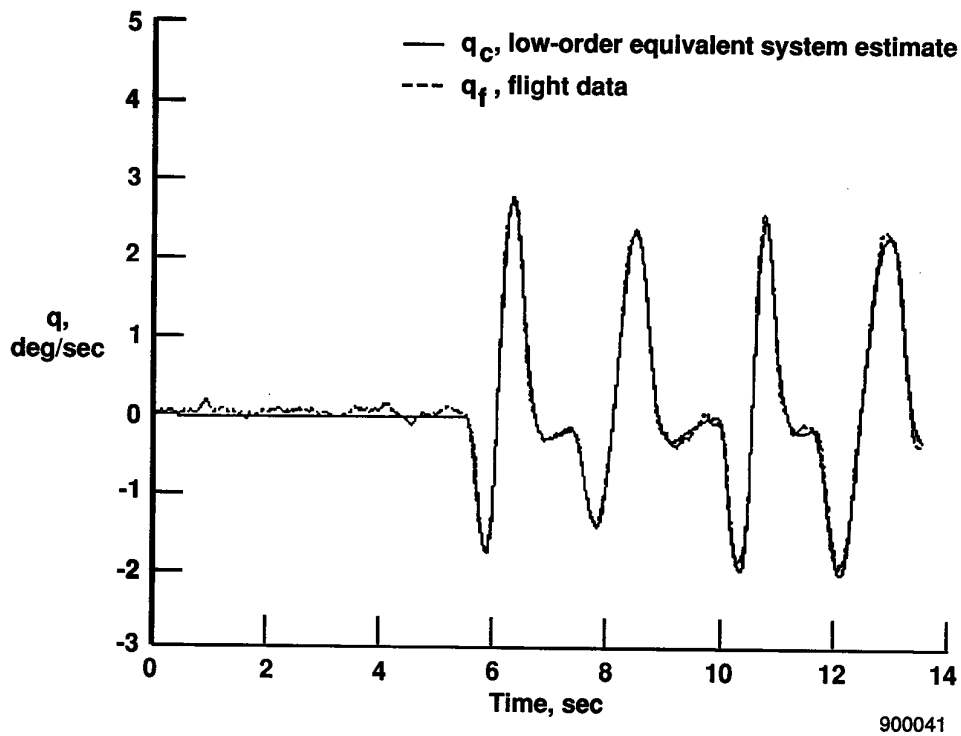
(b) Pitch rate.
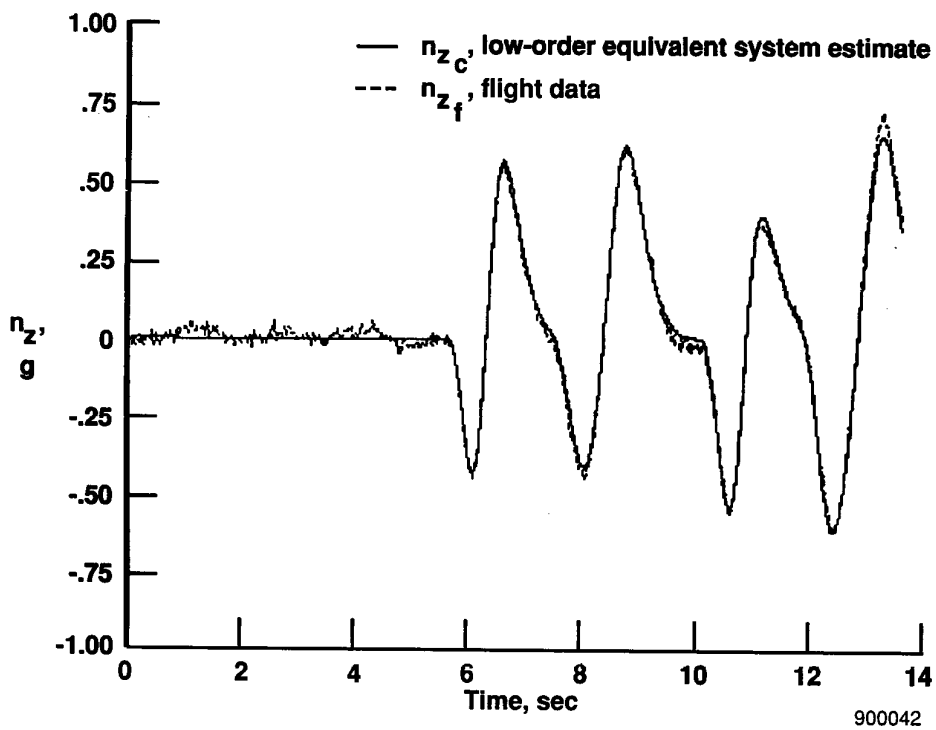
(c) Normal acceleration.

Fig. 5 Concluded.

19

(a) Angle of attack.

900043

(b) Pitch rate.

900044
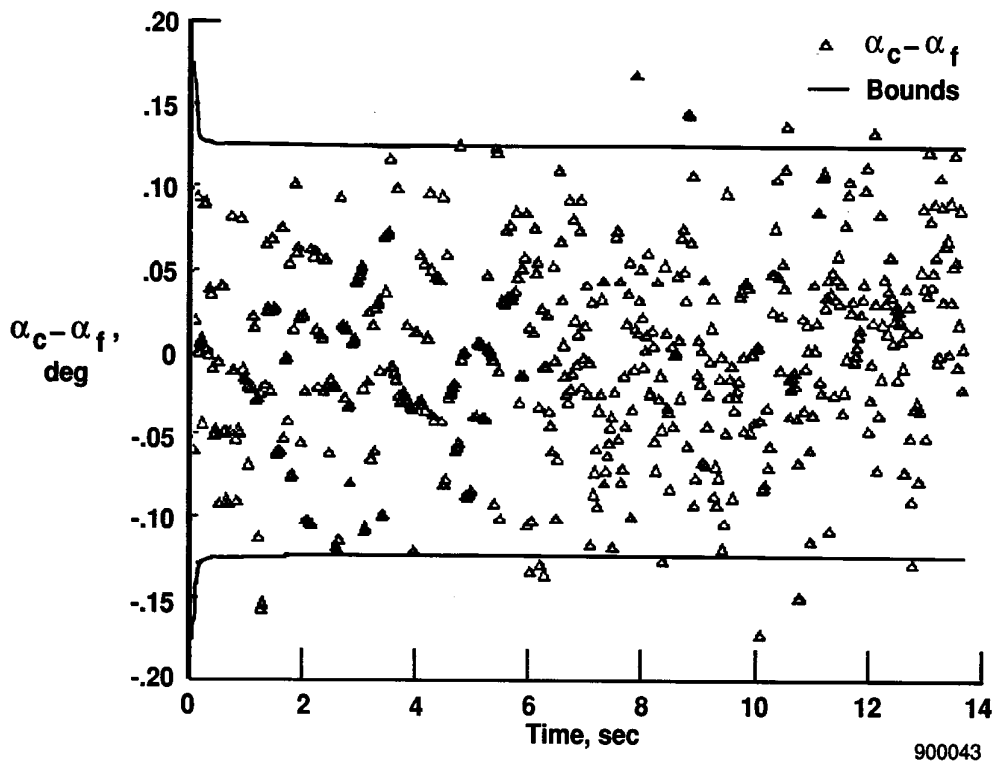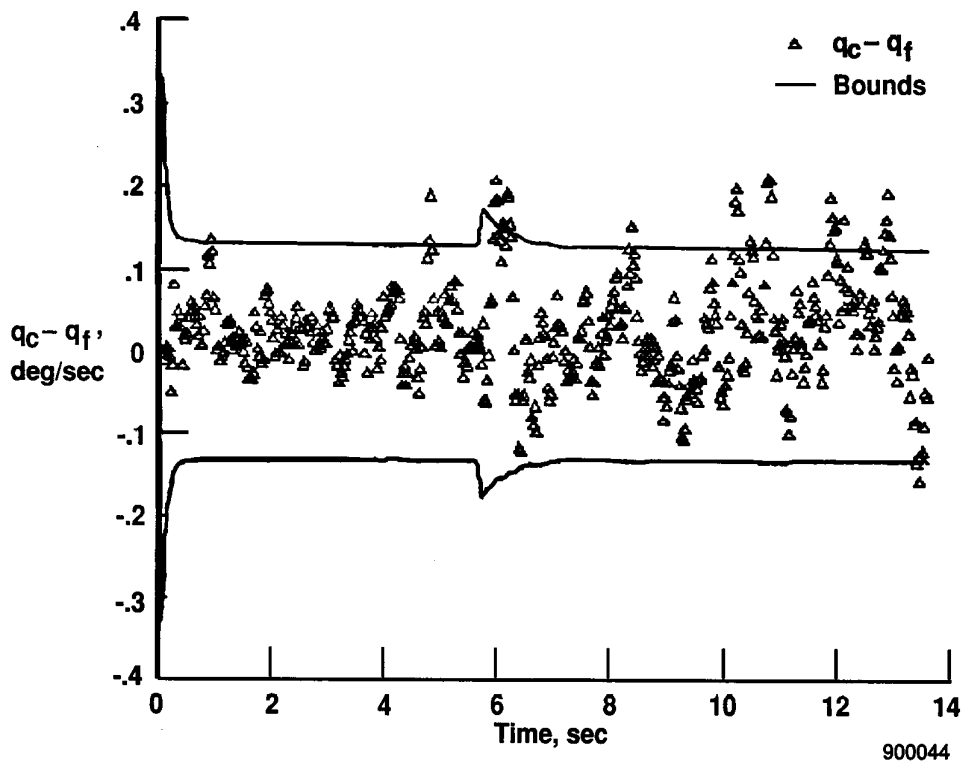
Fig. 6 Innovations for flight data identification.

20
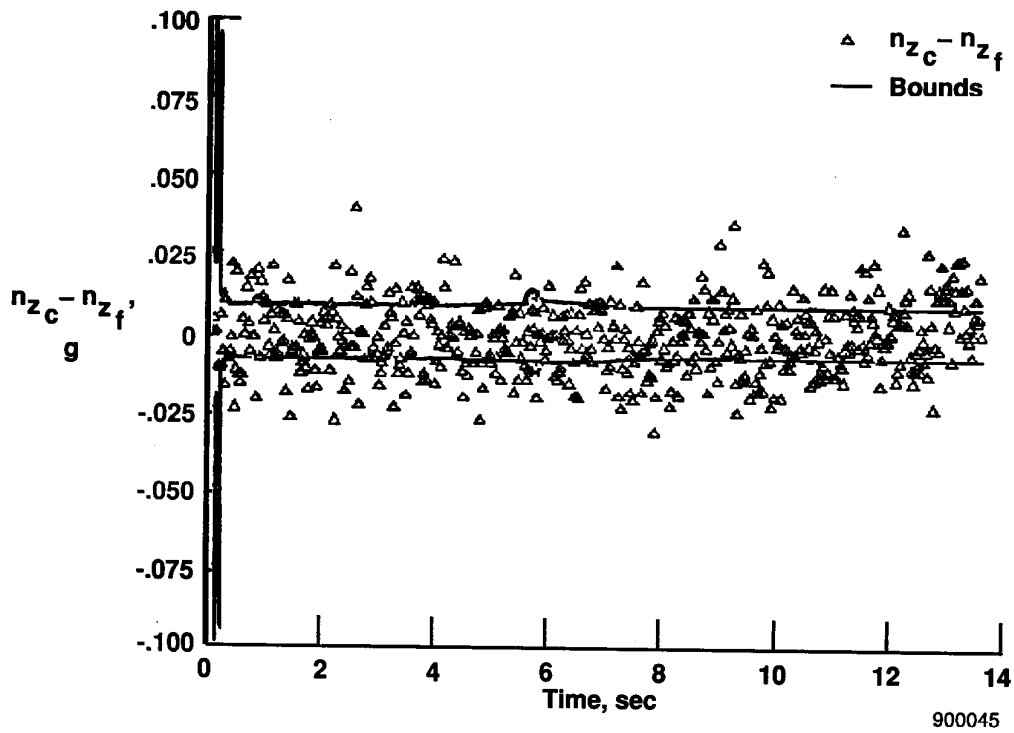
(c) Normal acceleration.

Fig. 6 Concluded.
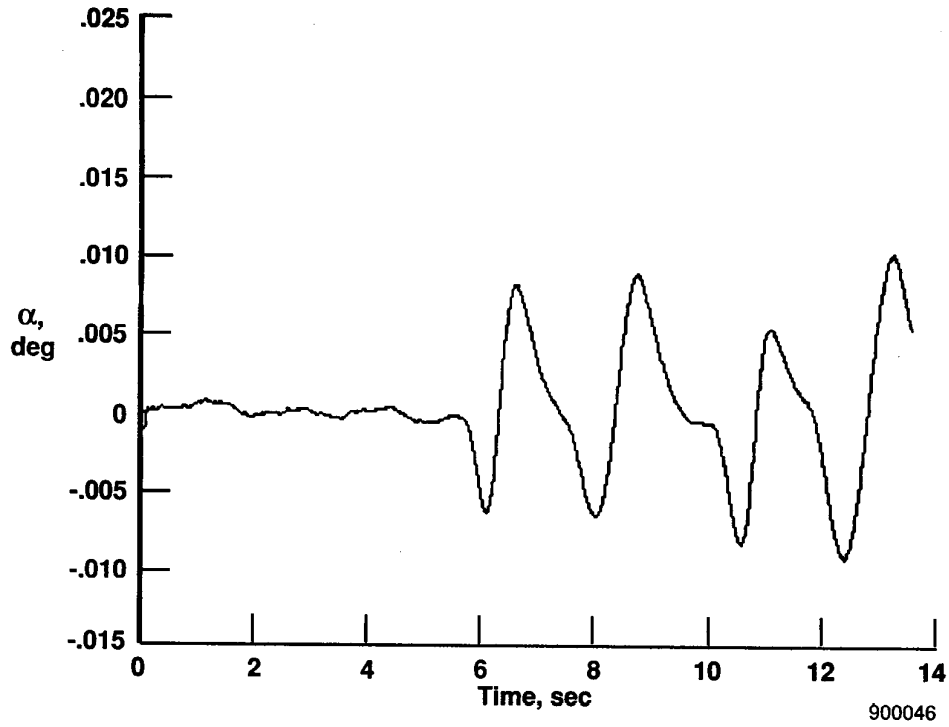
(a) Angle of attack.

Fig. 7 Estimated state time histories for flight data identification.

21

900047

(b) Pitch rate.

900048
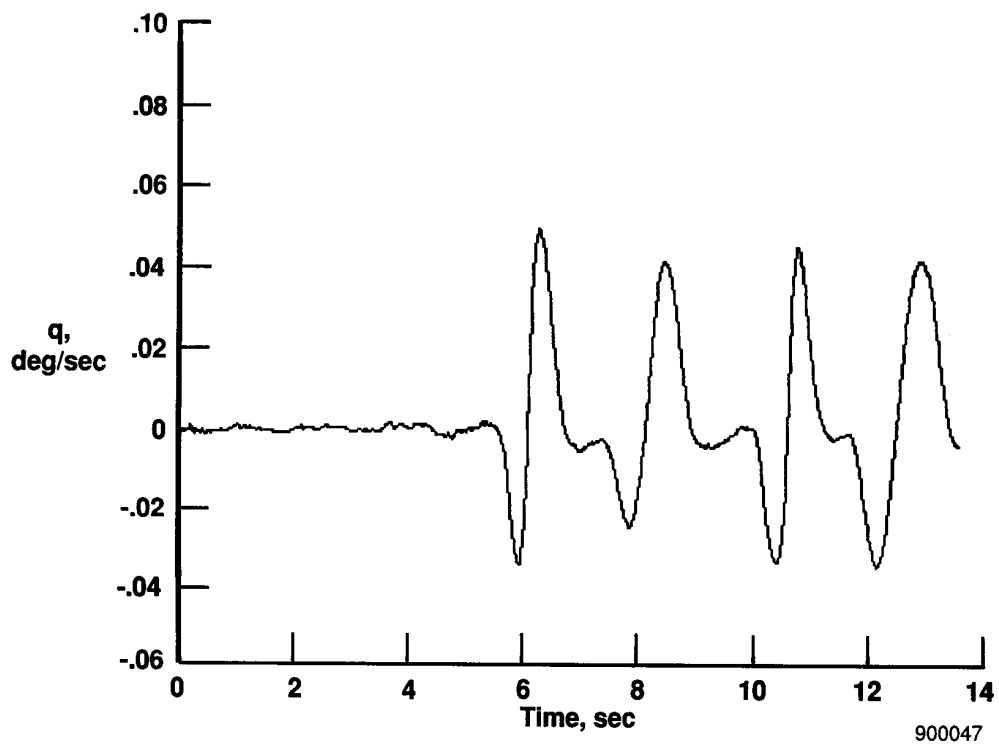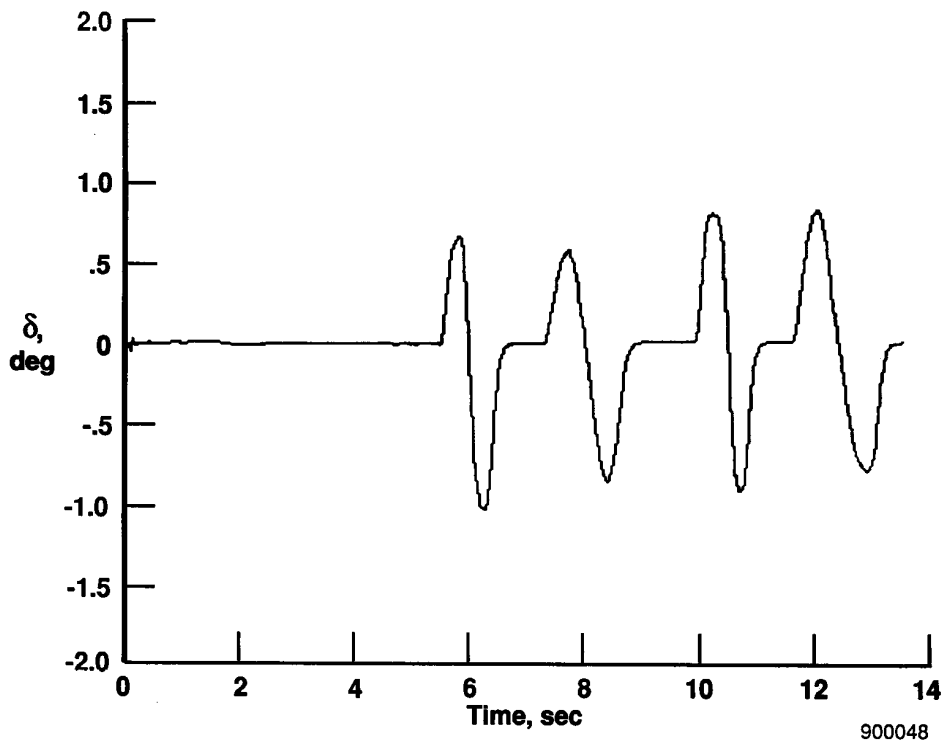
(c) Psuedo control surface deflection.

Fig. 7 Continued.

(d) L_α.

(e) M_α.

Fig. 7 Continued.

23

(f) L_δ.

900051

(g) M_δ.

900052

Fig. 7 Continued.

24
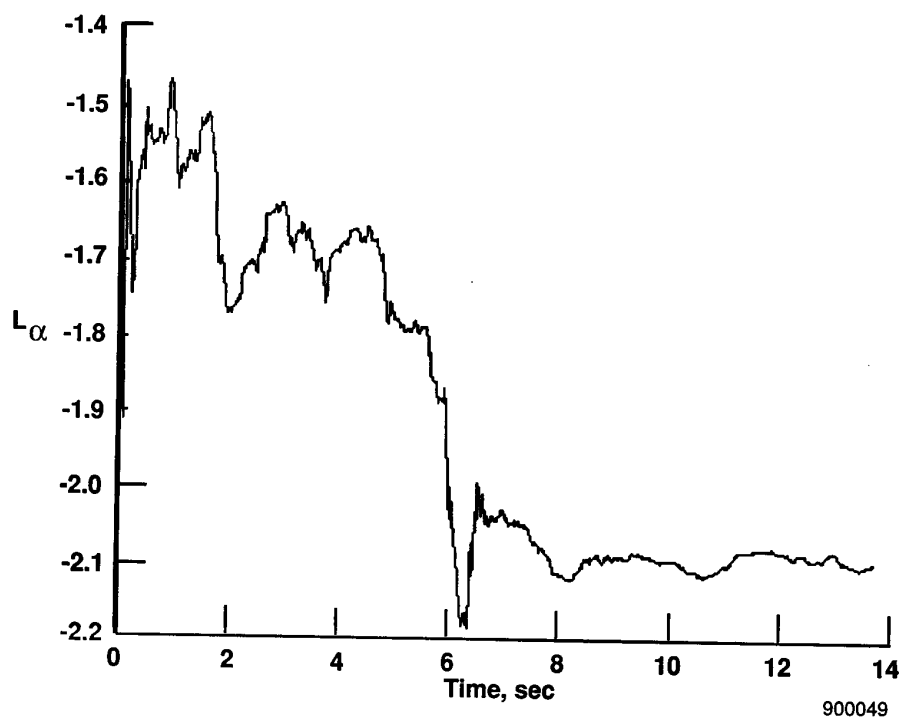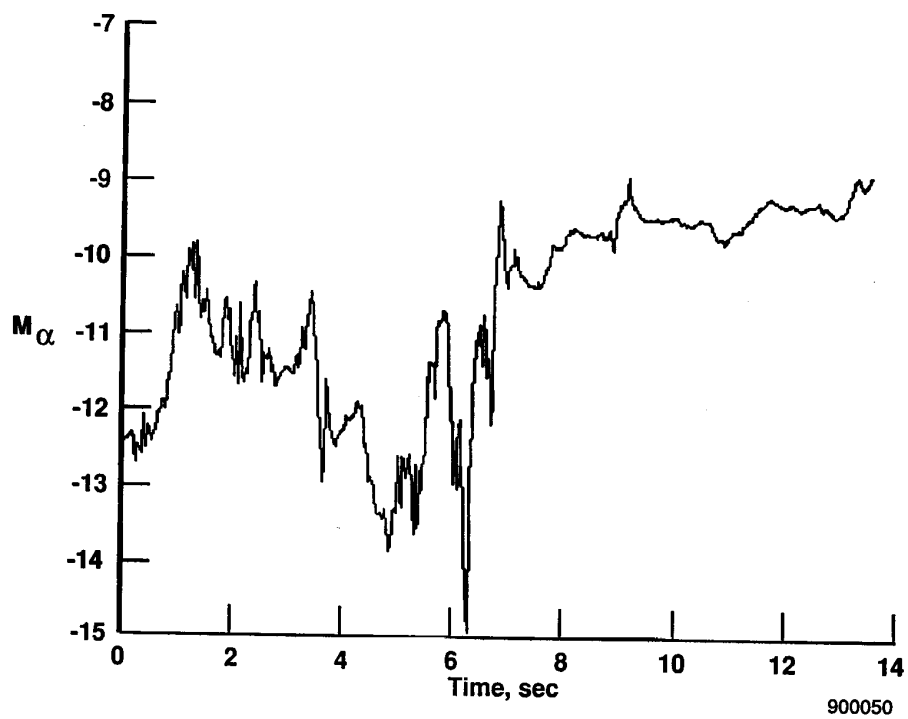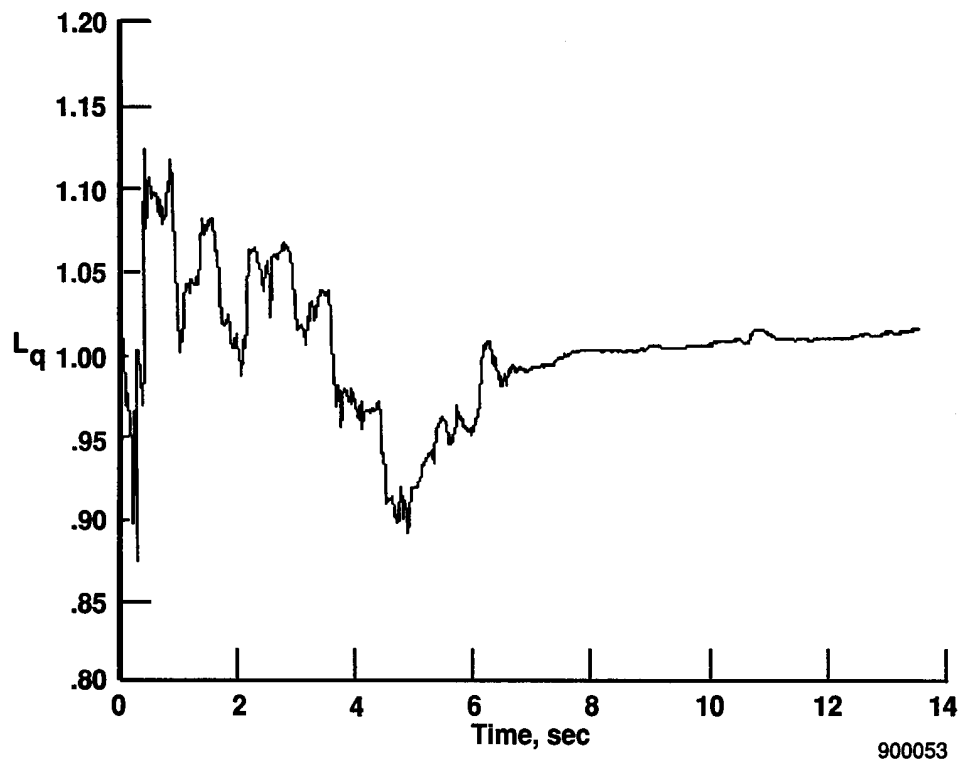
(h) L_q.
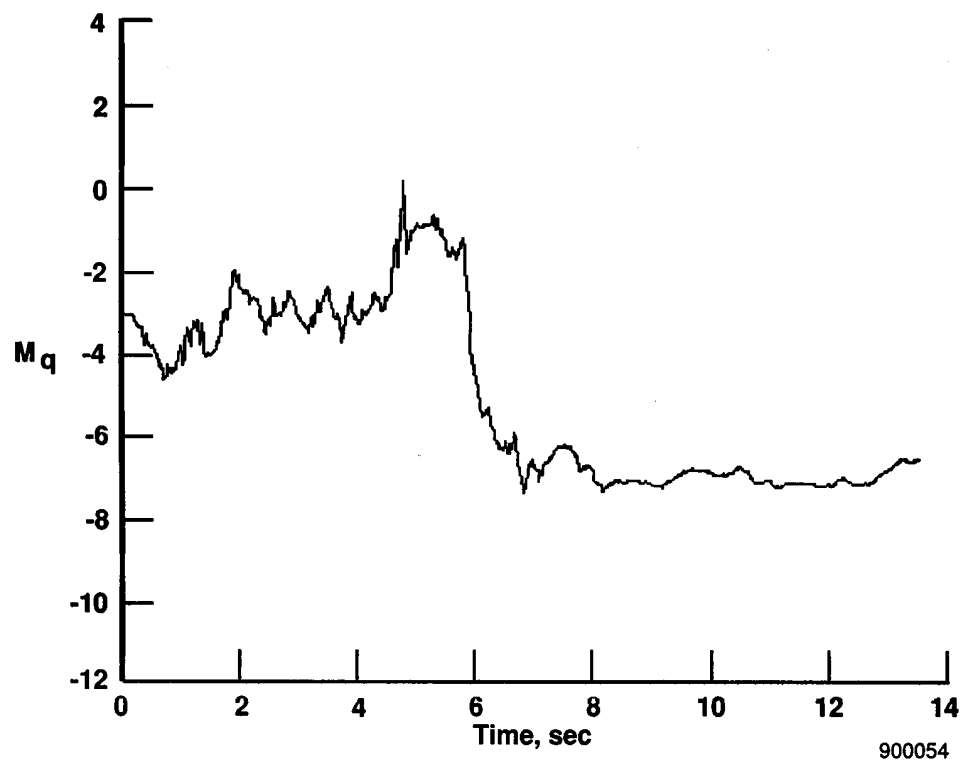
(i) M_q.

Fig. 7 Continued.

25

(j) $\frac{1}{\tau}$.

900055

(k) L_0.
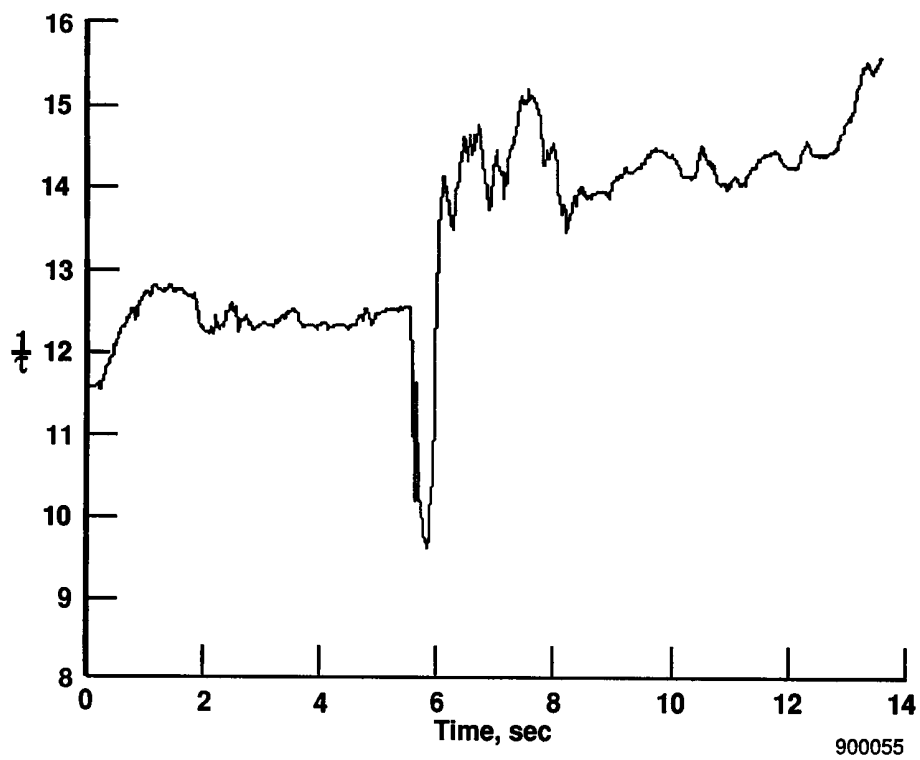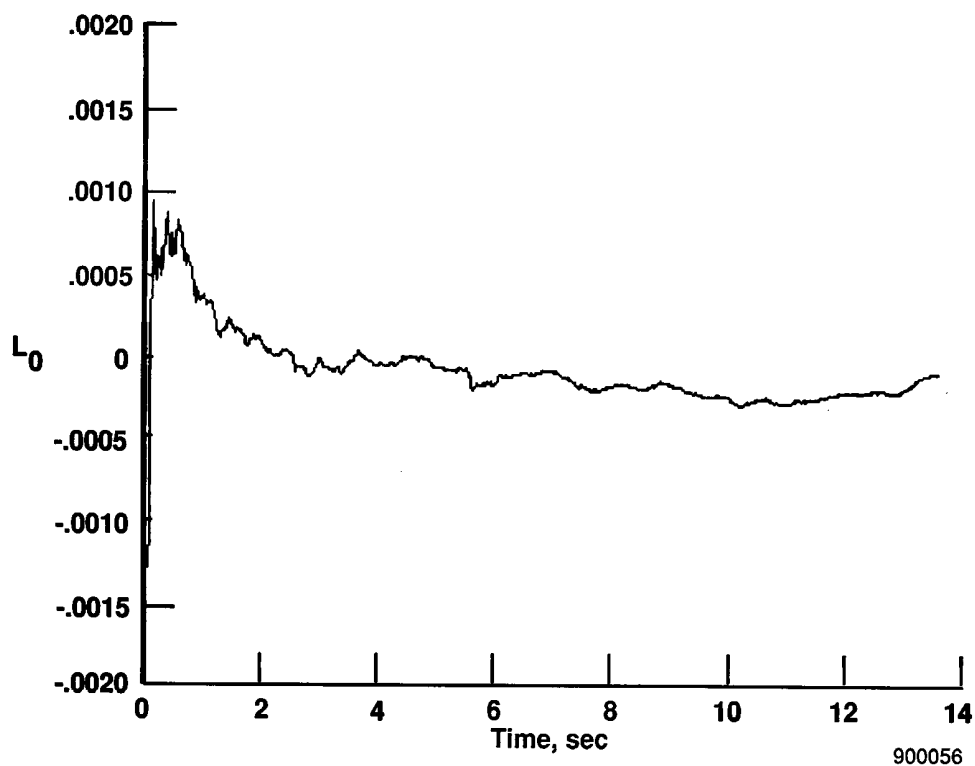
900056

Fig. 7 Continued.

(l) M_0.

(m) δ_0.
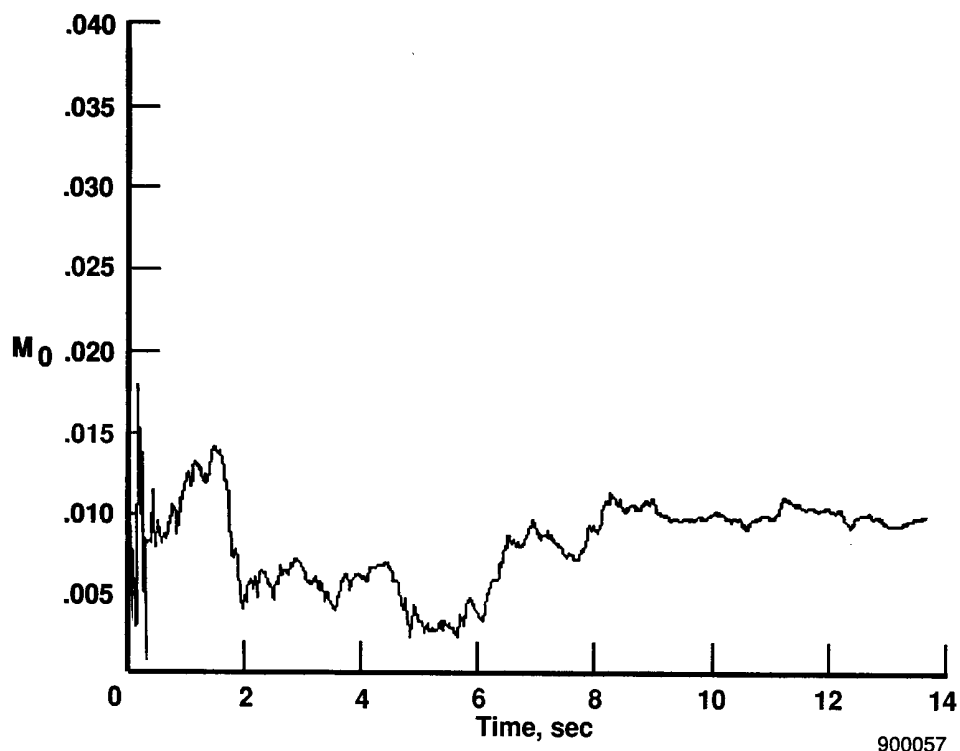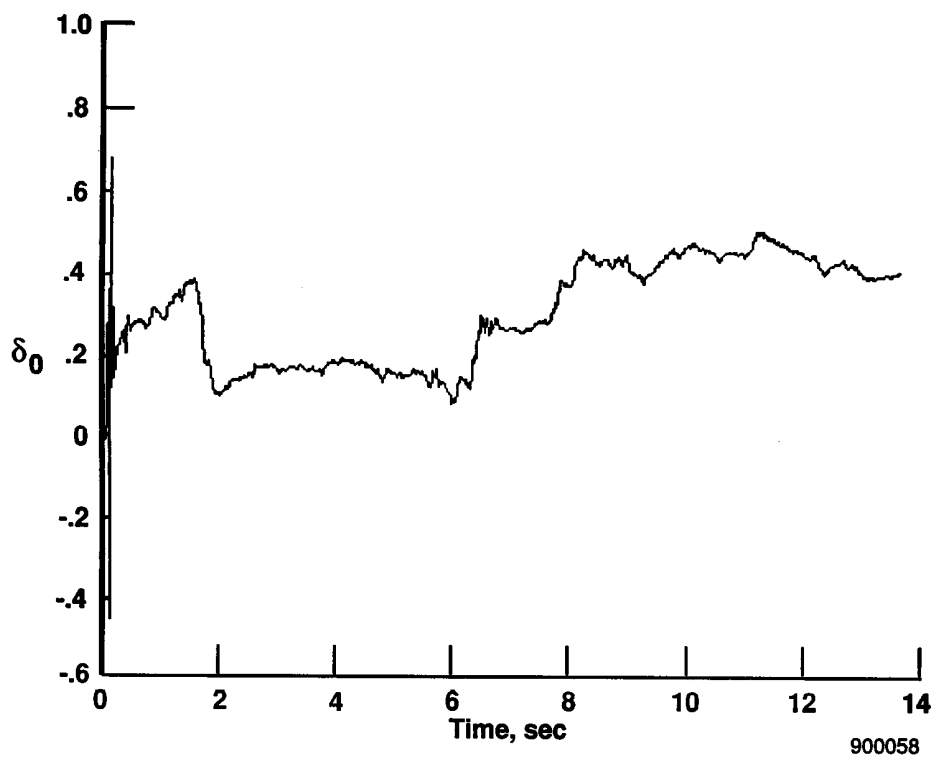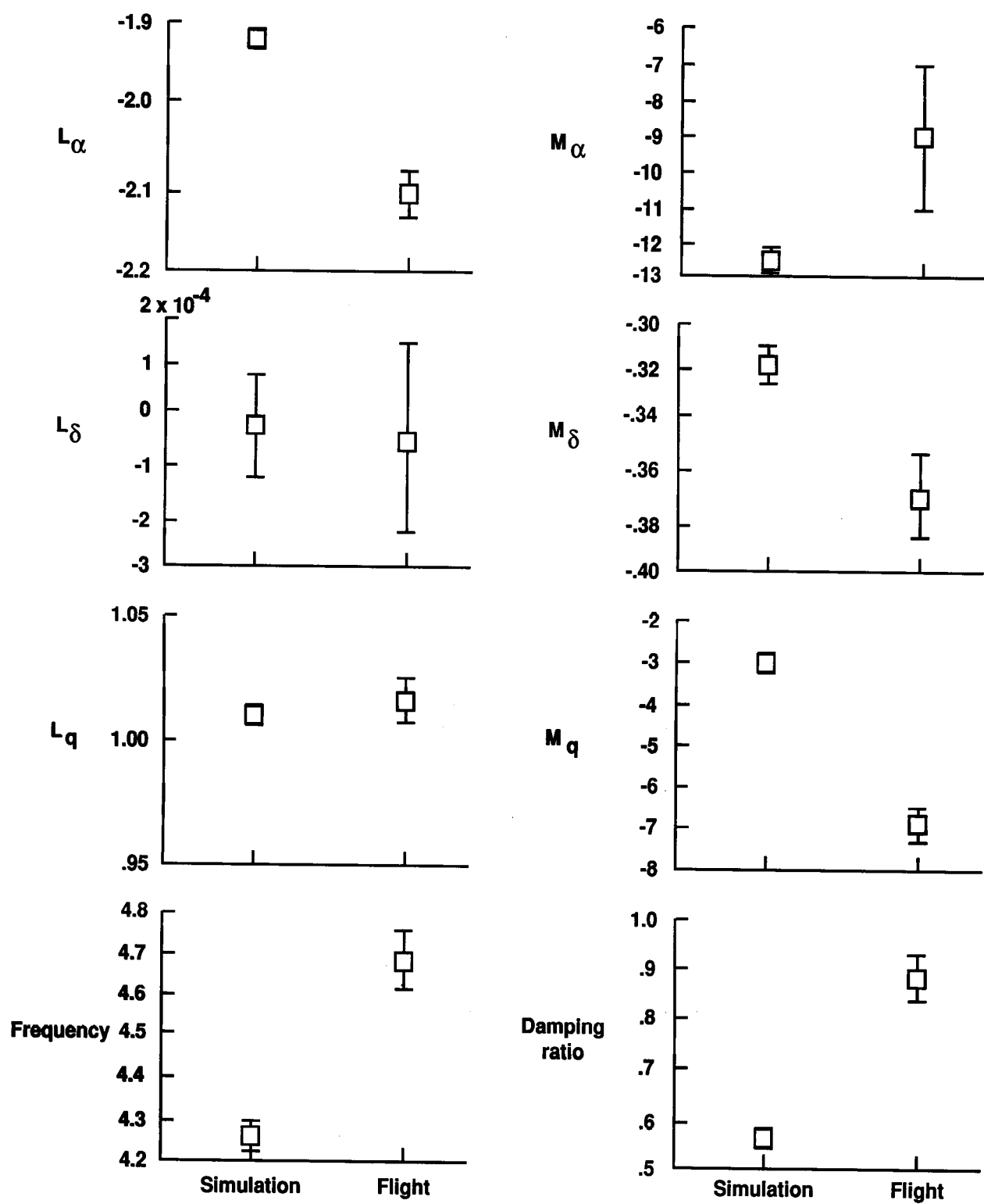
Fig. 7 Concluded.

Fig. 8 Simulation results compared with flight data.

900059

28

(a) L_α.

(b) M_α.
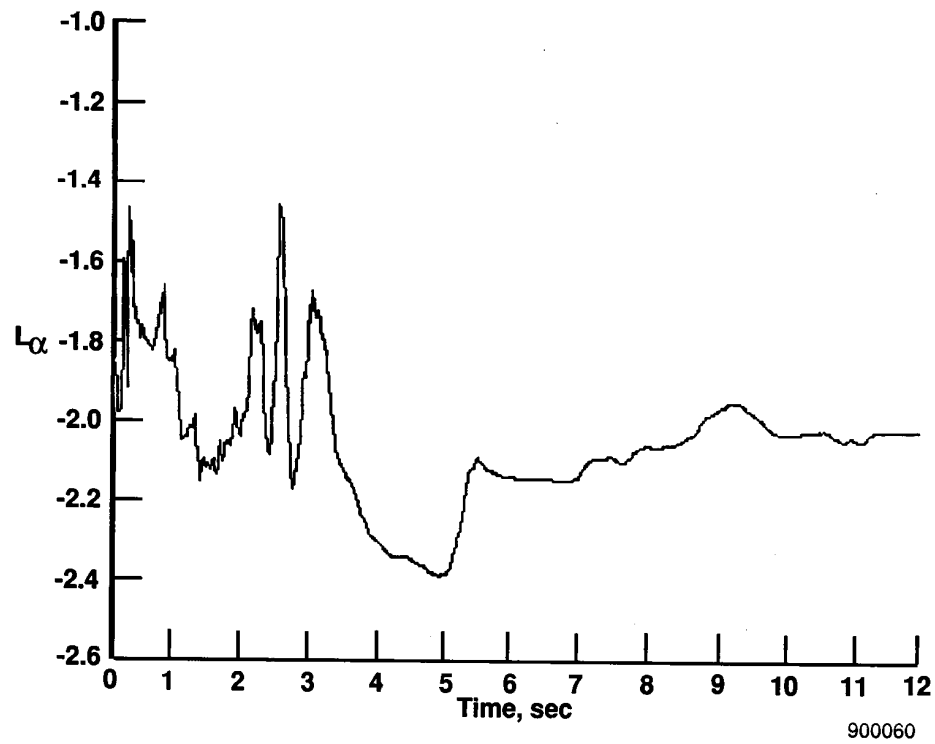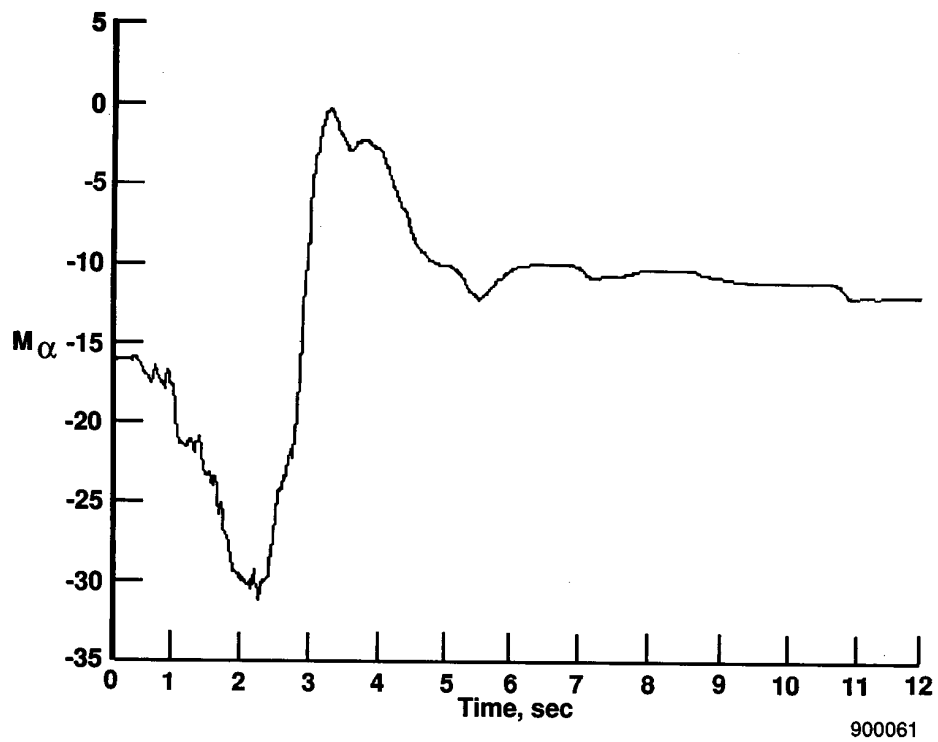
Fig. 9 Estimated state time histories for input with data spike.

29

(c) L_δ.

900062

(d) M_δ.

900063

Fig. 9 Continued.

30
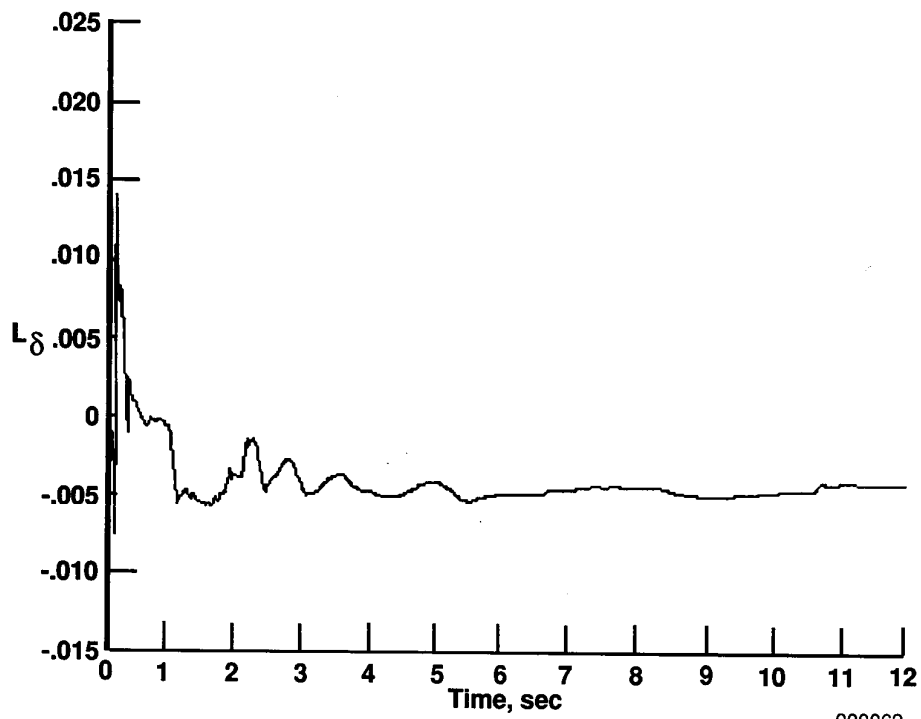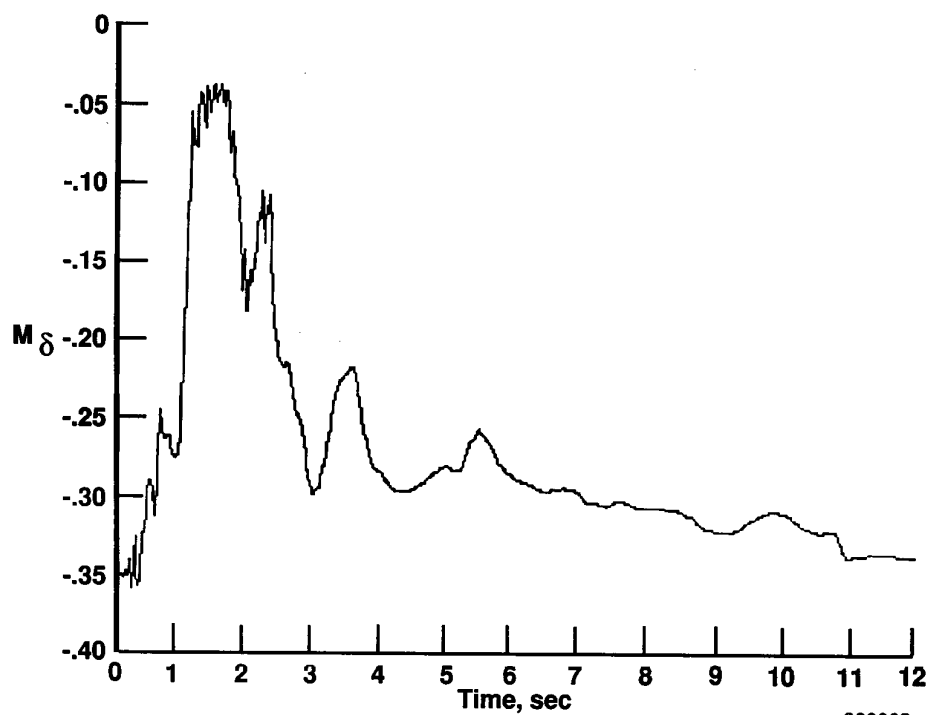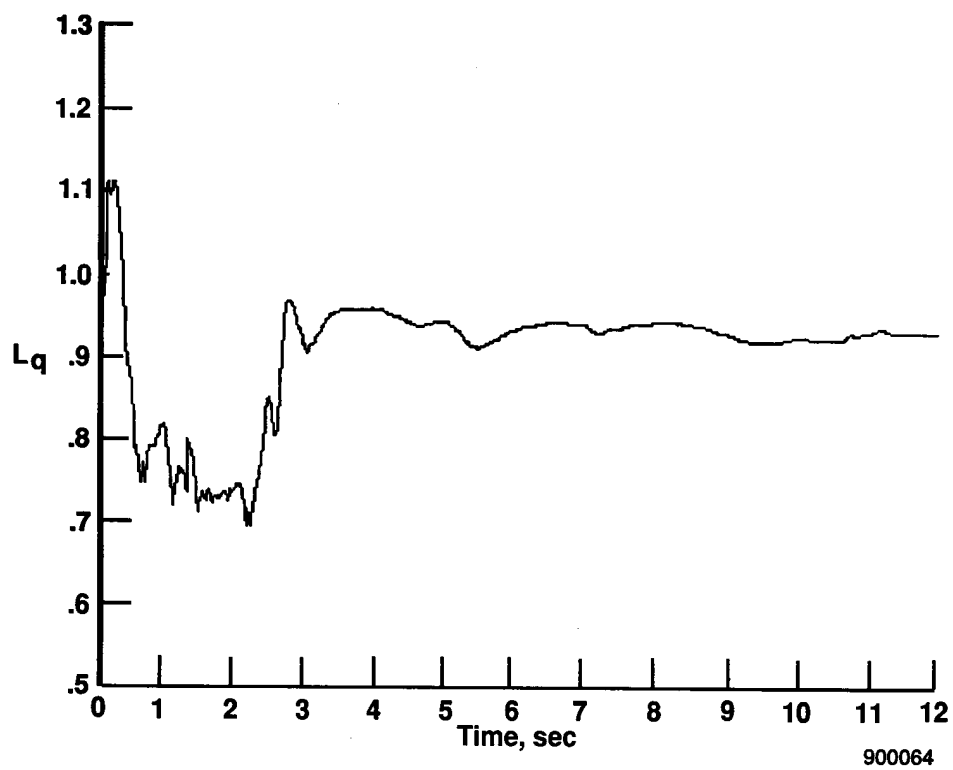
(e) L_q.
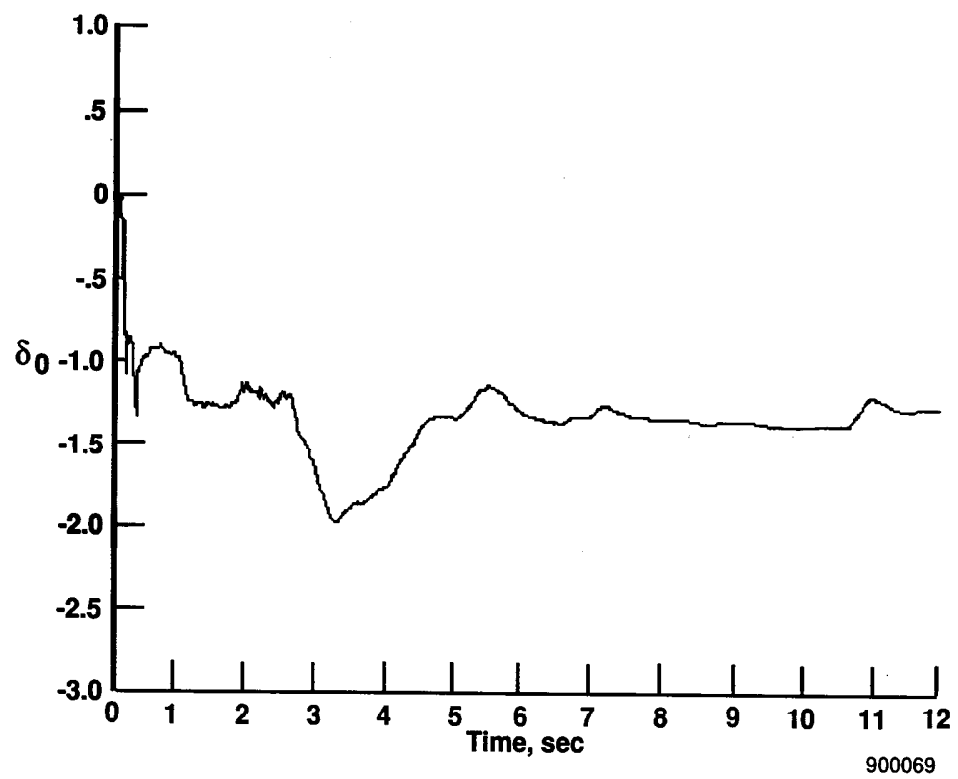

(f) M_q.

Fig. 9 Continued.

(g) $\frac{1}{\tau}$.

900066

(h) L_0.

900067

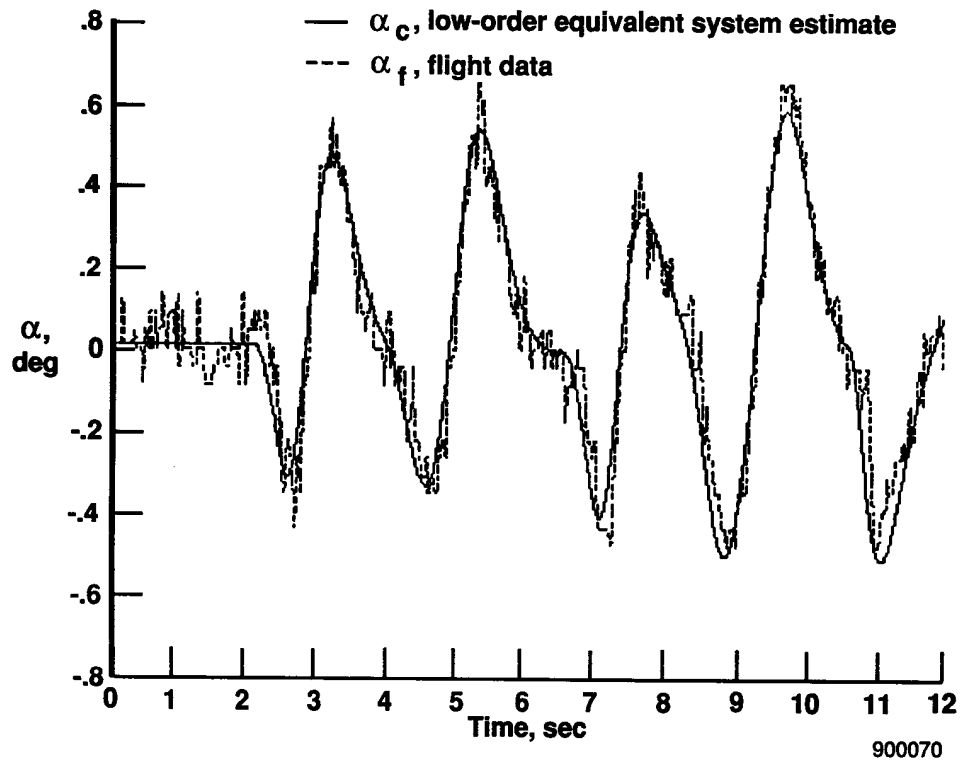Fig. 9 Continued.

32

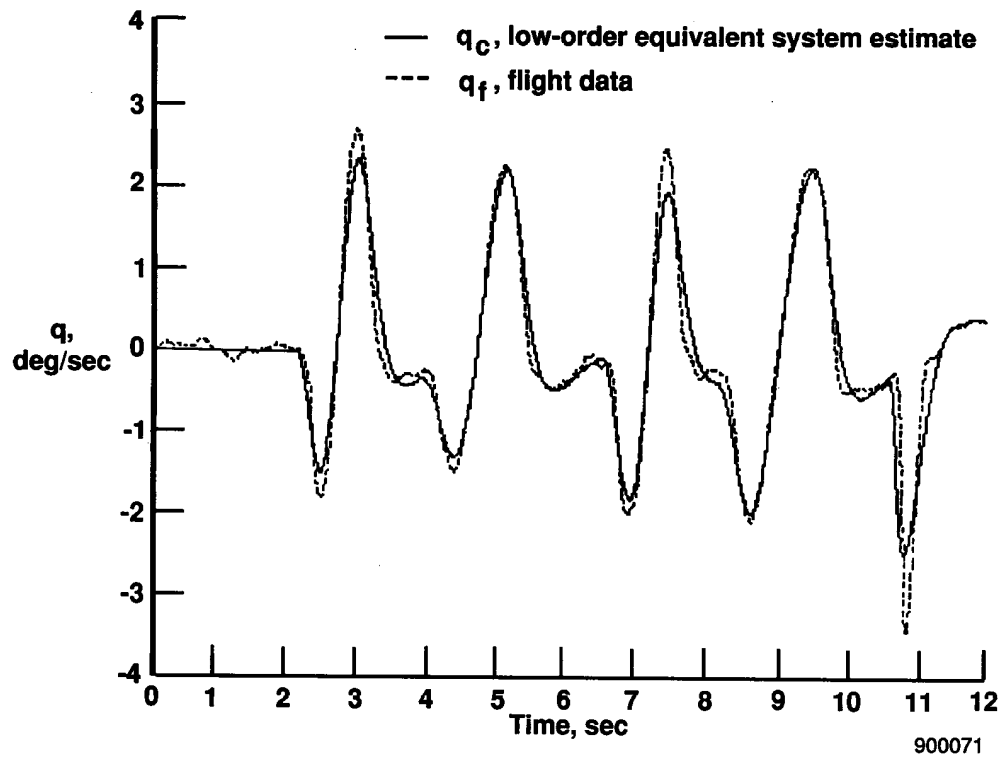(i) M_0.

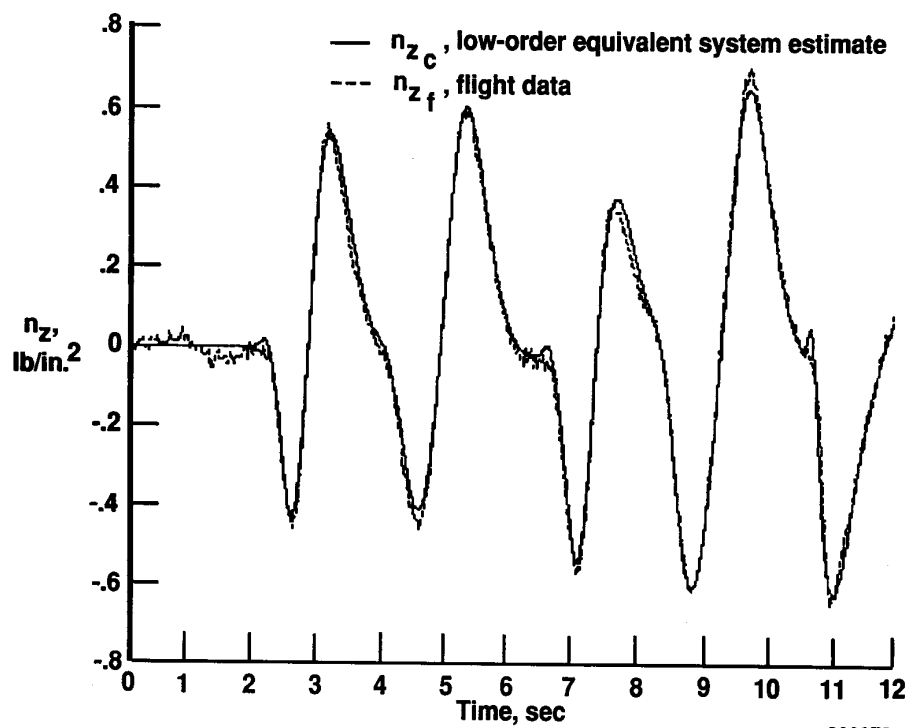(j) δ_0.

Fig. 9 Concluded.

33

(a) Angle of attack.

900070

(b) Pitch rate.

900071
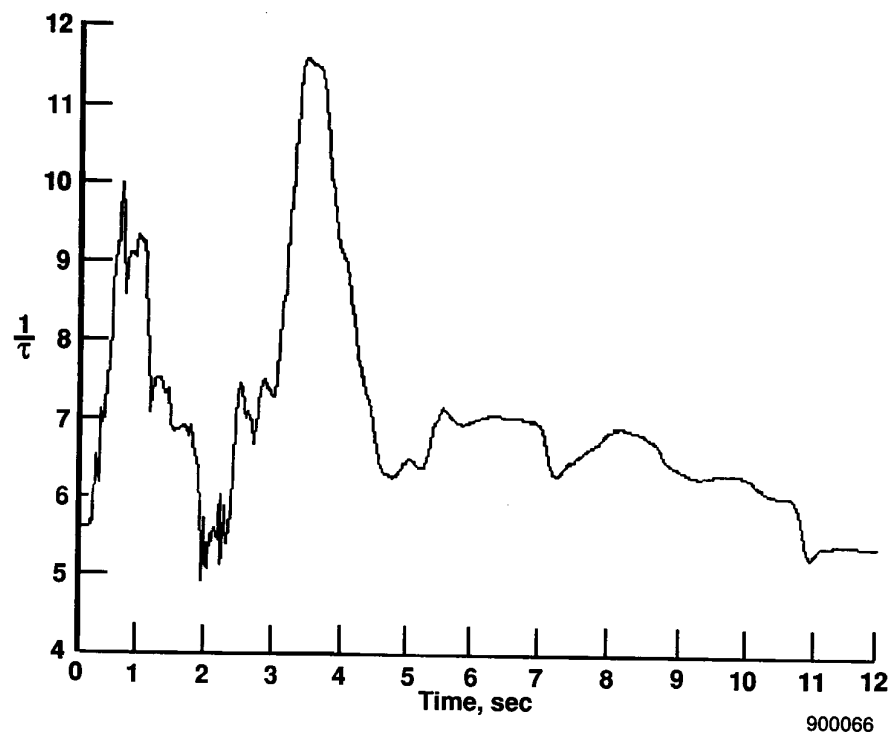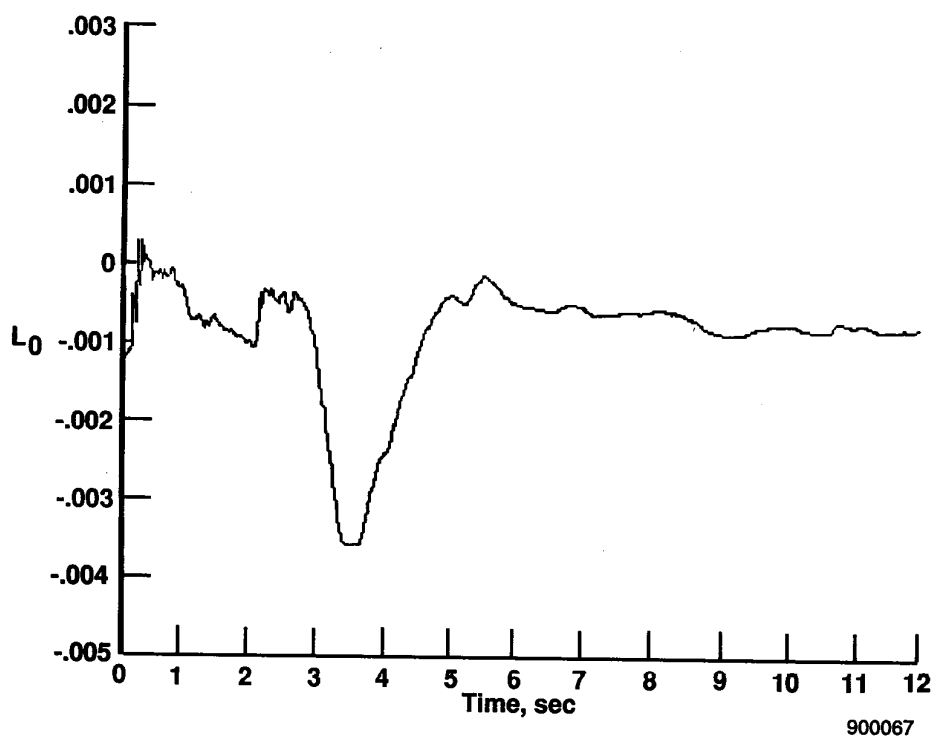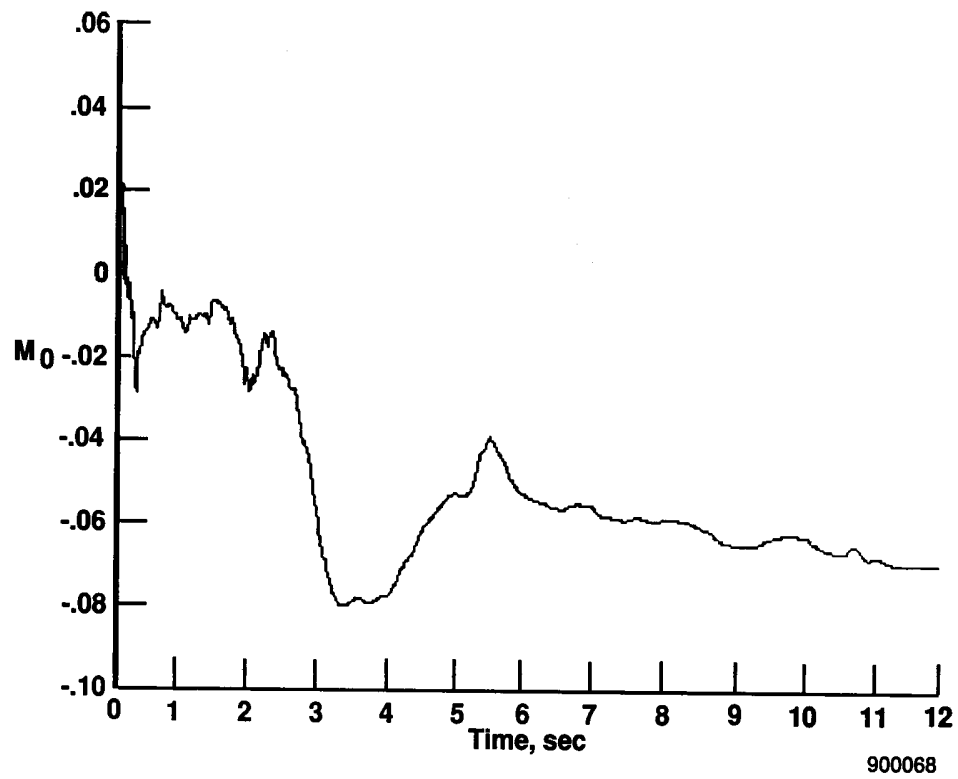
Fig. 10 Low-order equivalent system response compared with flight data (perturbation quantities) for input with data spike as a function of time.

34

(c) Normal acceleration.

Fig. 10 Concluded.

Report Documentation Page

1. Report No. NASA TM-101722	2. Government Accession No.	3. Recipient's Catalog No.
4. Title and Subtitle Estimating Short-Period Dynamics Using an Extended Kalman Filter		5. Report Date June 1990
		6. Performing Organization Code
7. Author(s) Jeffrey E. Bauer and Dominick Andrisani		8. Performing Organization Report No. H-1625
		10. Work Unit No. RTOP 533-02-51
9. Performing Organization Name and Address NASA Ames Research Center Dryden Flight Research Facility PO Box 273, Edwards,, CA 93235-0273		11. Contract or Grant No.
		13. Type of Report and Period Covered Technical Memorandum
12. Sponsoring Agency Name and Address National Aeronautics and Space Administration Washington, DC 20456-3191		14. Sponsoring Agency Code

15. Supplementary Notes

Prepared as AIAA 90-1277 for presentation at the AIAA/SFTE/SETP 5th Biannual Flight Test Conference, Ontario, CA, May 21–24, 1990.

16. Abstract

In this paper, an extended Kalman filter (EKF) is used to estimate the parameters of a low-order model from aircraft transient response data. The low-order model is a state space model derived from the short-period approximation of the longitudinal aircraft dynamics. The model corresponds to the pitch rate to stick force transfer function currently used in flying qualities analysis. Because of the model chosen, handling qualities information is also obtained. The parameters are estimated from flight data as well as from a six-degree-of-freedom, nonlinear simulation of the aircraft. These two estimates are then compared and the discrepancies noted. The low-order model is able to satisfactorily match both flight data and simulation data from a high-order computer simulation. The parameters obtained from the EKF analysis of flight data are compared to those obtained using frequency response analysis of the flight data. Time delays and damping ratios are compared and are in agreement. This technique demonstrates the potential to determine, in near real time, the extent of differences between computer models and the actual aircraft. Precise knowledge of these differences can help to determine the flying qualities of a test aircraft and lead to more efficient envelope expansion.

17. Key Words (Suggested by Author(s)) Kalman filter, Low-order equivalent model, Near-real-time, Parameter estimation, X-29A airplane	18. Distribution Statement Unclassified-Unlimited Subject Category - 05

19. Security Classif. (of this report) Unclassified	20. Security Classif. (of this page) Unclassified	21. No. of Pages 38	22. Price AO3